Contents list available at CBIORE journal website

International Journal of Renewable Energy Development

Journal homepage: https://ijred.cbiore.id

Research Article

Methodology for the selection and optimal sizing of standalone PV/Wind energy systems with battery storage under resource availability constraints

Guétinsom Jean Kafando, Daniel Yamegueu Nguewo*, Sani Moussa Kadri

Laboratoire Energies Renouvelables et Efficacité Energétique, Institut International d'Ingénierie de l'Eau et de l'Environnement (2iE), Rue de la Science, Ouagadougou, Burkina Faso

Abstract. Access to electricity remains a major challenge in sub-Saharan Africa, particularly in rural areas where grid extension is often costly and unviable. Standalone photovoltaic (PV) and/or wind power systems with battery storage represent a promising solution, yet they still face technical and economic barriers, especially related to sizing and storage costs. This paper proposes an innovative methodology for the selection and optimal sizing of such systems, integrating a predictive battery aging model based on the analysis of real charge/discharge cycles using the Rainflow algorithm and Miner's rule. The methodology relies on four main techno-economic performance indicators: the Loss of Power Supply Probability (LPSP), the Levelized Cost of Energy (LCOE), the Capacity Factor (CF) of a wind turbine, and the Weighted Index of Complementarity and Productivity (WICP). It accounts for available resources, the user's hourly consumption profile, and local climatic conditions. The methodology is applied to a rural site in Nagréongo, Burkina Faso. The results show that only a PV/battery system is technically and economically viable, while wind and hybrid configurations are excluded due to low wind potential, as indicated by CF and WICP values below acceptable thresholds. Furthermore, the analysis demonstrates that the optimal system configuration strongly depends on the hourly consumption profile, even for identical daily energy demands. Finally, comparison with the classical intuitive sizing method and the widely used HOMER Pro software shows that the proposed approach reduces the LCOE by more than 50% and about 20%, respectively, by accurately accounting for real battery aging, demand variability, and system idle periods.

Keywords: Standalone System, PV/Wind Systems, Battery Aging, Sizing, Optimization, Weighted Index of Complementarity and Productivity.

Received: 2nd Sept 2025; Revised: 17th March 2026; Accepted: 4th May 2026; Available online: 9th May 2026

1. Introduction

In 2024, according to the International Energy Agency (IEA), the number of people without access to electricity worldwide is estimated at nearly 750 million (International Energy Agency 2024a). Yet, the seventh Sustainable Development Goal (SDG 7), adopted in 2015 by the United Nations General Assembly, aims to ensure universal access to reliable, sustainable, affordable, and modern energy services by 2030 (United Nation 2025). Among this population, 80% live in sub-Saharan Africa and more strikingly, 80% of those without electricity in the region reside in rural areas (International Energy Agency 2024b). In these areas, extending the power grid is often very costly and economically unviable due to the remoteness of villages and the low population density (Diouf and Miezan 2024). To address this situation, the deployment of standalone solar and/or wind power systems with electrochemical energy storage is considered one of the major solutions for achieving SDG 7(Onyeanusi 2025). Indeed, the sub-Saharan Africa region benefits from high solar potential and a few moderately windy sites, according to the IEA (International Energy Agency 2022c). Moreover, this solution aligns with global carbon neutrality trajectories over the next few decades, in line with the Paris Agreement, which aims to limit global warming to below 2°C (Nationally Determined Contributions 2024). However, despite the numerous advantages of this approach and its strong recommendation by the IEA for remote areas, several challenges remain. These systems, powered by variable renewable sources, still pose technical reliability issues even with storage and face economic accessibility constraints. In Africa, these barriers are especially significant because most rural populations have limited incomes, restricting their ability to invest in such solutions (Diouf and Miezan 2024). These difficulties stem particularly from the high cost of system components, especially storage batteries, and from often inadequate system sizing (Kafando, Yamegueu and Houdji 2024). Undersizing results in frequent power shortages for users, while oversizing leads to unnecessary economic burdens. Various sizing methods and tools for these systems have been reported in the literature. They can be grouped into two main categories: traditional methods (intuitive, iterative, analytical, probabilistic, etc.) and artificial intelligence-based methods (genetic algorithms, particle swarm optimization, etc.) (Kafando, Yamegueu and Houdji 2024). Among traditional methods, two remain widely

* Corresponding author

Email: daniel.yamegueu@2ie-edu.org (D.Y. Nguewo)

https://doi.org/10.61435/ijred.2026.61740

ISSN: 2252-4940/© 2026.The Author(s). Published by CBIORE

used for the sizing of photovoltaic (PV) / wind systems with storage: the intuitive method and the iterative method. The intuitive approach uses monthly or annual average solar irradiance and/or wind speed data to size the stand-alone PV/wind generator (Busaidi *et al.* 2015). Battery storage capacity is often determined empirically, based on assumed autonomy periods ranging from 2 to 5 days, which may lead to oversizing and increased costs. For instance, some studies recommend autonomy periods of 2 to 9 days (Cardona and López 1998) or 3 to 5 days (Ridha *et al.* 2020). The iterative approach aims to improve upon the intuitive method by using time-series data (solar irradiation, wind speed, and load profiles). It generally relies on indicators such as the Loss of Power Supply Probability (LPSP) and the Levelized Cost of Energy (LCOE) to assess system reliability and economic feasibility (Busaidi *et al.* 2015). This method involves iterating over key system parameters (PV size, wind generator size, and storage capacity or autonomy) to identify all configurations meeting a target LPSP value set by the user and then selecting the one with the lowest LCOE as optimal (Diaf et al. 2008a). However, this approach still often assumes long autonomy durations (1 to 5 days). Moreover, it uses nominal battery lifespans provided by manufacturers, which are defined for regular charge/discharge cycles. In systems powered by intermittent renewable sources (solar and wind), these cycles are irregular, leading to potential inaccuracies in battery lifetime estimates. For example, in (Diaf *et al.* 2008a, b), the iterative approach was applied to determine the optimal configuration of a hybrid PV/wind system with battery storage to meet energy demand in several Corsican localities (Calvi, Ajaccio, Cap Corse, etc.). These studies showed that the available resource level influences the system configuration. However, the optimal autonomy periods found ranged from 2 to 3 days in some locations and 4 to 6 days in others, which remain relatively high. Battery lifetime was fixed at 4 years. Similarly, in (Kaabeche, Belhamel and Ibtiouen 2011), a study optimizing a hybrid PV/wind/battery system under various LPSP targets (1%, 3%, and 5%) considered a battery lifetime of 4 years and autonomy between 1 and 5 days. Similar works have been reported in (Boumechta and Kaabeche 2015; Derai and Kaabeche 2016; Othman *et al.* 2022; Bakelli *et al.* 2025), but without integrating charge/discharge cycle analysis to estimate battery lifetime under real operating conditions. Despite the extensive literature on the sizing of standalone and hybrid renewable energy systems, a clear gap remains in the integration of realistic battery aging models into the sizing and optimization process. Most existing approaches rely on fixed or nominal battery lifetimes, independent of the actual operating conditions, load variability, and irregular charge–discharge cycles induced by intermittent renewable sources. This simplification may lead to significant inaccuracies in both system reliability assessment and LCOE estimation, particularly in rural off-grid applications where batteries represent a major share of the total system cost. Unlike most existing sizing approaches, the methodology proposed in this work explicitly links system sizing, battery aging, and economic performance within a unified framework. By accounting for the temporal variability of both renewable resources and load demand, as well as the real degradation behavior of batteries under irregular cycling, the proposed approach enables a more realistic and economically relevant optimization of standalone and hybrid renewable energy systems. This article thus aims, first, to propose a methodology for the selection and optimal sizing of PV and/or wind systems with battery storage, and second, to validate this methodology through a comparison of its results on a case of study with those obtained using the traditional intuitive method and the HOMER software, which is one of the most widely used tools in that domain. The proposed methodology considers several factors: resource availability, fluctuation, and complementarity; the temporal distribution of user energy demand; and real-world battery aging. The goal is to optimize system component sizes (PV generator, wind generator, and batteries) to improve economic accessibility while accurately estimating the LCOE, given that battery lifetime plays a key role in its calculation. The methodology is based on an energy model, a battery aging model, and several performance indicators, including the wind turbine Capacity Factor (CF), the Temporal Complementarity Index (TCI), the Weighted Index of Complementarity and Productivity (WICP), the LPSP, and the LCOE. Furthermore, using an iterative process, it will first identify the most suitable system (PV and/or wind with storage) for a given site, based on available solar and wind resources, and then determine the optimal system configuration by balancing LPSP and LCOE. The main contributions of this study can be summarized as follows: (i) the development of a decision-oriented framework for selecting the most appropriate standalone renewable energy system (PV, wind, or hybrid) based on resource availability and complementarity indicators; (ii) the integration of a predictive battery aging model based on Rainflow cycle counting and Miner's rule into the sizing and optimization process; (iii) the evaluation of the impact of hourly consumption profiles on system configuration, reliability, and LCOE; (iv) a comparative validation of the proposed methodology against the classical intuitive sizing method and the widely used HOMER Pro software under realistic local conditions.

2. Methods

2.1. Description of the PV/Wind system with storage

Figure 1 presents the basic architecture of the hybrid system used in our sizing approach. It mainly consists of a photovoltaic (PV) generator, a wind turbine and a battery bank for storing or delivering energy. Several power converters manage the energy flows within the system. The DC/DC converter adjusts the voltage of the PV generator to that of the DC bus. The other DC/DC converter transforms the voltage of the bus to that of the DC Load. The AC/DC converter transforms the alternating current generated by the wind turbine into direct current compatible with the DC bus. The bidirectional DC/DC converter enables charging and discharging of the batteries according to system requirements. Finally, the DC/AC converter converts the DC bus current into AC power to supply the loads. This configuration is well suited for remote areas that benefit from both solar and wind resources due to the complementary nature of the two sources (Jurasz *et al.* 2024; Lv and Tang 2025): solar energy covers daytime needs, while wind energy takes over at night or during cloudy weather. Depending on the available site resources, the system can be simplified. If the wind potential is low, the wind turbine and its converter are removed from the system. Conversely, if solar irradiance is insufficient, the PV generator and its converter are excluded. From an electrical architecture standpoint, three configurations are possible: AC bus, DC bus, or hybrid AC/DC architecture (Ishaq *et al.* 2022). While AC buses are widely used, they require strict synchronization of sources in terms of frequency, voltage, and phase, which increases system complexity, cost, and instability (Brenna, Lazaroiu and Tironi 2006). Hybrid architectures face the same AC-side constraints and add energy

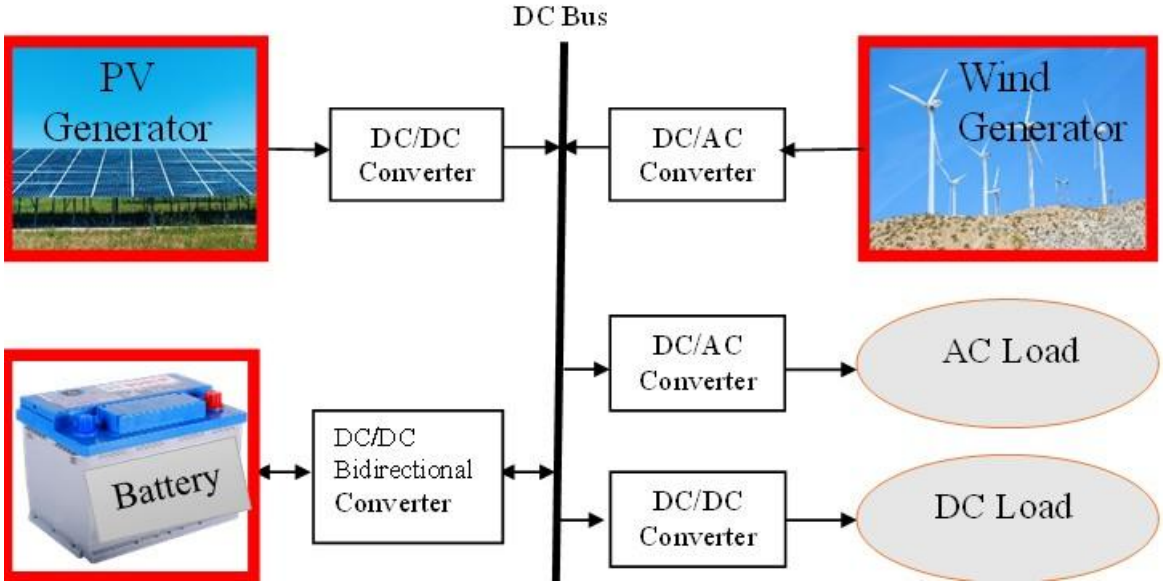

Fig 1. Configuration of the adopted PV/ Wind/Storage System

losses due to cross-conversions. Therefore, our approach favors a DC bus architecture, which is better suited for DC sources and storage, simpler, more efficient, and ideal for remote areas (HOMER Energy by UL 2023**)**.

2.2. Energy model of system

Modeling the main components of the previously described system is a fundamental step for its optimal sizing.

2.2.1. PV Generator Model

The PV generator is modeled by its instantaneous output power $P_{PV}(t)$ at each time step *t*, as expressed in Equation (1). This power depends not only on the PV generator's peak power P_P , but also on the solar irradiance $G_I(t)$ received at time *t* on the surface of the modules tilted at an angle β with respect to the horizontal, and on the module temperatureT_{mod}, which in turn depends on the ambient temperature $T_a(t)$, as shown in Equation (2) (Diaf *et al.* 2008b ; Kotb *et al.* 2020 ; Kadri *et al.* 2022)**.**

$$P_{PV}(t) = P_p * \frac{G_I(t)}{G_{ref}} * f_{loss} * \left(1 - \gamma * \left(T_{mod}(t) - T_{ref}\right)\right) \quad (1)$$

$$T_{mod}(t) = T_a(t) + \frac{G_I(t)}{G_{ref}} * \left(T_{NOCT} - T_{ref}\right) \quad (2)$$

Where: P_P : Rated peak power of the PV generator (W_p), $G_{ref}$and T_{ref} : Reference values of irradiance and temperature (1000 W/m² and 25°C) , f_{loss} : Soiling factor (This factor ranges between 0 and 1. However, a value of 0.85 is very commonly used in the literature.), accounting for power losses due to dust, γ : Temperature coefficient (for silicon cells the range is 0.004–0.006/°C. In this study 0.004/°C is used.), $T_{mod}(t)$: Instantaneous module temperature (°C), T_{NOCT} : Module temperature under 800 W/m² irradiance and 20°C ambient temperature

2.2.2. Wind Generator Model

The wind generator is modeled by its instantaneous output power $P_{WT}(t)$ at each time *t* (in watts), as represented by Equation (3). This power depends not only on the nominal power of the selected wind turbines, but also on the wind speed impacting the turbine blades, which in turn depends on both the installation height and ground surface roughness, as expressed in Equation (4) (Diaf *et al.* 2008b)**.**

$$P_{WT}(t) = \begin{cases} P_{WTR}\left(\frac{v^2(t) - {v_{IN}}^2}{{v_R}^2 - {v_{OUT}}^2}\right) & \text{if } v_{IN} < v(t) < v_R \\ P_{WTR} & \text{if } v_R \le v(t) < v_{OUT} \\ 0 & \text{if } v(t) \le v_D \text{ and } v(t) > v_{OUT} \end{cases} \quad (3)$$

$$v(t) = v_{ref}(t)\left(\frac{H}{H_{ref}}\right)^{\psi} \quad (4)$$

Where: P_{WTR} and v_R are rated power and rated wind speed of the wind generator (W, m/s), $v_{IN}$and v_{OUT} Cut-in and cut-out wind speeds of the turbine (m/s), $v(t)$ Instantaneous wind speed at height H (in meters) at time t (m/s), ψ Wind shear exponent representing ground surface roughness; it ranges from 0.10 to 0.40 (0.14 is used in this study. This value is a standard value commonly used for low-roughness surfaces, such as open rural areas, flat fields, or grassy zones with no significant obstacles), $v_{ref}(t)$: Instantaneous wind speed at reference height, H_{ref} at time t (m/s)

2.2.3. Battery Bank Model

The battery bank is modeled by its storage capacity S_{BAT}in ampere-hours (Ah) and its state of charge $SOC(t)$ in watt-hours (Wh) at each time t, as given by Equations (6) and (7). The storage capacity model is based on the classical formulation shown in Equation (5), in which the daily energy demand E_D(Wh/day) and the number of autonomy days N_D(days), are respectively replaced by the average hourly load E_H (Wh/hour), given by Equation (8), and the number of autonomy hours N_H

(hour or h). In addition to these substitutions, a linear correction of the capacity as a function of the annual average ambient temperature $Ta_{moy}$is introduced using the coefficient k_{cap}, which typically ranges from 0.005 to 0.01/°C for lead-acid or lithium-ion batteries (DiOrio et al. 2015; Saxena *et al.* 2015), to account for capacity variation with temperature. Indeed, literature shows that battery capacity is temperature-dependent (DiOrio *et al.* 2015; Saxena et al. 2015), while standards or manufacturers usually provide capacity values at a reference temperature Ta_{ref} of 20°C or 25°C. The state of charge depends not only on the energy surplus or deficit $\Delta P(t)$ (positive in case of surplus, negative in case of deficit), as given by Equation (9), but also on the self-discharge coefficient ϕ, which depends on battery technology. It is considered as 40%, 25%, and 20% per month for lead-acid, nickel-cadmium, and lithium batteries, respectively (Korsaga *et al.* 2018).

$$S_{BAT}^{CLA} = \frac{E_D * N_D}{U_{BAT} * DOD_{MAX} * \eta_{BAT}} \quad (5)$$

$$S_{BAT} = \frac{E_H * N_H}{U_{BAT} * DOD_{MAX} * \eta_{BAT}} * \left(1 - k_{cap}\left(Ta_{ref} - Ta_{moy}\right)\right) \quad (6)$$

$$SOC(t) = SOC(t-1)\phi + \Delta P(t)\, \Delta t\, \eta_{BAT} \quad (7)$$

$$E_H = \frac{\sum_{t=1}^{24}(P_{CH}(t))}{(24 - N_{Hoff})} \quad (8)$$

$$\Delta P(t) = P_{PV}(t)\eta_{DC-DC} + P_{WT}(t) * \eta_{AC-DC} - P_{CH}(t)\frac{1}{\eta_{DC-AC}} \quad (9)$$

With E_D and N_D: User's average daily energy need (Wh/day) and number of autonomy days, E_H and N_H: User's average hourly load (Wh/h) and battery autonomy duration (h), U_{BAT}andη_{BAT}: Voltage (V) and efficiency (%) of the battery bank, DOD_{MAX}: Maximum depth of discharge of the batteries, $P_{CH}(t)$: Power demand of the user at each time *t* during the day, N_{Hoff}: Number of non-active hours (zero power demand) in a day, Δt: Simulation time step (1 hour), $P_{PV}(t)$ and $P_{WT}(t)$: Power output (in W) from the PV and wind generators at time t , $\eta_{DC/DC}$, $\eta_{AC/DC}$ and η_{DC-AC}: Efficiencies of the DC/DC, AC/DC, and DC/AC converters, respectively, The battery bank voltage U_{BAT} also corresponds to the system operating voltage U_{SYST}, which is selected based on the user's daily energy demand (Bhatia 2008) as follows:

$U_{BAT} = U_{SYST} = 12V$ for $E_D \leq 1.5$ kWh/day

$U_{BAT} = U_{SYST} = 24V$ for 1.5 kWh/day $< E_D \leq 4$ kWh/day

$U_{BAT} = U_{SYST} = 48V$ for $E_D > 4$ kWh/day

2.3. Battery aging model

Battery lifetime is a key parameter in the economic analysis of standalone PV/wind systems with energy storage. However, system designers often rely on the battery lifetime provided by the manufacturer, which is typically based on specific conditions involving regular charge-discharge cycles and a fixed ambient temperature of 20°C or 25°C. In standalone PV / wind systems with storage, the cycling behavior of batteries is irregular due to the fluctuating nature of renewable sources. To account for this variability in the system sizing process, a battery aging calculation model previously proposed in (Layadi and Champenois 2014), and based on manufacturer data, has been integrated into the iterative approach developed in this study to predict battery lifetime. To estimate battery life, the process illustrated in Figure 2 is followed. In this process, the battery's state of charge (SOC) profile obtained from the physical system simulation over a one-year period is first processed by the Rainflow cycle counting algorithm, which converts it into a series of depths of discharge (DOD_j), where j ranges from 1 to n, and n is the total number of cycles counted. Next, Miner's rule is applied to assess the cyclic aging rate (T_{VC}), as defined in Equation (10), i.e., the damage caused by each counted cycle. This is calculated using Equation (11), referred to as the battery aging curve, which considers the effect of mean annual ambient temperature Ta_{moy}. The curve provided by manufacturers describes battery lifetime versus depth of discharge at a reference temperature Ta_{ref} (typically 20°C or 25°C) and is expressed by Equation (12).

$$T_{VC} = \frac{1}{N_{Cj(DOD_j)}} \quad (10)$$

$$N_C(DOD) = N_C(DOD)_{Ta_{ref}}\, exp\left(-\theta(Ta_{moy} - Ta_{ref})\right) \quad (11)$$

$$N_C(DOD)_{Ta_{ref}} = a + b\, exp(c * DOD) + d\, exp(e * DOD) \quad (12)$$

Where θ is a temperature sensitivity coefficient, typically taken as 0.0693 °C^{-1}, derived from the assumption that battery life is halved for every 10 °C increase above the reference temperature (DiOrio *et al.* 2015; Saxena *et al.* 2015). a, b, c, d are empirical constants obtained by fitting the manufacturer's cycle life data using MATLAB software.

Finally, the battery lifetime (in years) is derived from the annual degradation rate T_{VA}, using Equation (13).

$$T_{VA} = 100 * \sum_{j=1}^{n} \frac{1}{N_{Cj(DOD_j)}} \text{ (in \%)} \quad (13)$$

If, for instance, T_{VA}=25%, this implies a battery lifetime of 4 years.

Miner's rule states that for a given depth of discharge, the damage caused by a single cycle is equal to the inverse of the

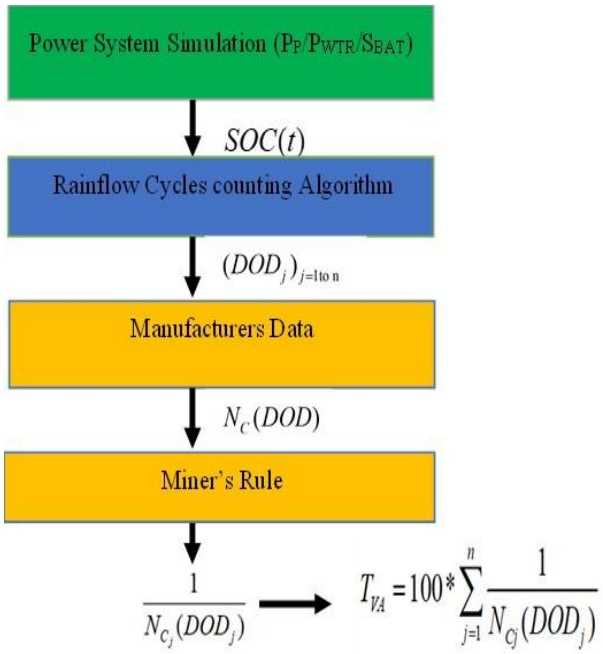

Fig 2 . Battery Aging Calculation Model

number of cycles associated with that depth (Layadi and Champenois 2014).

2.4. System performance criteria

2.4.1. Wind Site Viability Criterion

Nowadays, the wind energy industry offers small wind turbines (with rated power < 20 kW) to meet electricity and water pumping needs in moderately or weakly windy areas. However, wind conditions in such areas are considered suitable for installing a given wind turbine only if its Capacity Factor (CF) exceeds 20%, according to the 2024 report of the Global Wind Energy Council (GWEC). This report states that the average capacity factor of wind turbines at viable sites generally ranges between 20% and 50% (Global Wind Energy Council 2024). The Capacity Factor, defined by Equation (14), depends not only on wind conditions (speed and consistency) but also on the characteristics of the selected wind turbine (Sedaghat et al. 2020; Jurasz et al. 2025). A low CF (< 20%) indicates insufficient wind resources, whereas a CF ≥ 20% reflects favorable wind conditions. Our approach integrates the Capacity Factor concept to assess the wind potential of a given site for wind turbine deployment.

$$CF = \frac{\int_{v_{IN}}^{v_{OUT}} P_{WT}(v) * f(v) dv}{P_{WTR_{ONE}}} \quad (14)$$

Where:

$P_{WTR_{ONE}}$is a one wind turbine rated power (in W), $f(v)$ is the probability density function, defined in Equation (15) and corresponding to the Weibull distribution, which is widely used in wind farm design software such as WasP, WindPro, etc., to approximate the frequency distribution of wind speeds (Carta, Ramírez and Velázquez 2009).

$$f(V) = \frac{k}{C}\left(\frac{V}{C}\right)^{k-1} exp\left[-\left(\frac{V}{C}\right)^{k}\right] \quad (15)$$

The shape and scale parameters k and C, defined in Equations (16) and (17), are dimensionless and dimensional (m/s), respectively. The shape parameter k describes the form of the wind speed distribution curve, while the scale parameter C reflects the wind quality at the site (Nsouandélé et al. 2017).

$$k = 1 + \frac{3.69}{IR^2} \quad (16)$$

$$C = \frac{V_{moy}}{\Gamma\left(1+\frac{1}{k}\right)} \quad (17)$$

The parameter IR, defined by Equation (18), is called the Irregularity Factor. It is the ratio between the mean of the cubed wind speed and the cube of the mean wind speed, providing insight into wind consistency (Nsouandélé *et al.* 2017).

$$IR = \frac{\frac{1}{N}\sum_{i=1}^{N} V_i^3}{V_{moy}^3} \quad (18)$$

Where Γ(x) is the Gamma function, defined as $\Gamma(x) = \int_0^{\infty} t^{x-1} e^t dt$ for all x.

2.4.2. Temporal Complementarity Criterion

The Temporal Complementarity Index (TCI), defined in Equation (19), is used to assess the temporal coordination between wind and solar power production. Its formulation here is based on a cosine similarity metric applied to the normalized hourly profiles of solar and wind generation, inspired by the work in (Beluco, De Souza and Krenzinger 2008; Canales *et al.* 2019; Jurasz *et al.* 2019). A TCI = 100% indicates perfect complementarity between solar and wind energy (i.e., when solar output is low, wind production is high, and vice versa), while a TCI = 0% reflects perfect synchronization, meaning poor complementarity. Complementarity is considered acceptable when TCI ≥ 50%.

$$TCI = \left(1 - \frac{\sum_{t=1}^{8760} P_{PV}^{norm}(t) * P_{WT}^{norm}(t)}{\sqrt{\sum_{t=1}^{8760}\left(P_{PV}^{norm}(t)\right)^2} * \sqrt{\sum_{t=1}^{8760}\left(P_{WT}^{norm}(t)\right)^2}}\right) * 100 \quad (19)$$

Where $P_{PV}^{norm}(t)$ and $P_{WT}^{norm}(t)$ are the normalized hourly profiles of solar and wind production, respectively, defined in Equations (20) and (21):

$$P_{PV}^{norm}(t) = \frac{G_I(t)}{G_{I_{MAX}}} \quad (20)$$

$$P_{WT}^{norm}(t) = \frac{P_{WT}(t)}{P_{WTR_{ONE}}} \quad (21)$$

Where:$G_I(t)$: Hourly global irradiance on a tilted surface (W/m²), $G_{I_{MAX}}$: Maximum annual irradiance value (W/m²), $P_{WT}(t)$: Hourly wind power output (W) , $P_{WTR_{ONE}}$: Rated power of the selected wind turbine (W).

2.4.3. Hybridization Relevance Criterion

Several studies have shown that the complementarity between variable renewable energy sources plays a key role in reducing power variability, storage requirements, and system costs (Jurasz *et al.* 2019; Jonasson and Temiz 2025). These previous studies provided a comprehensive review of the statistical correlations, metrics, and indices commonly used to assess both temporal and spatial complementarity between fluctuating resources such as solar, wind, and hydropower, including the fluctuation-based indices, the Temporal Complementarity Index (TCI) and the Pearson correlation coefficient, which remains one of the most widely used to indicate whether resources tend to compensate each other over time. The authors highlighted the diversity of indices, the lack of a common methodology, and the difficulty of decision-making for system designers.

Although indicators such as the fluctuation-based indices, the Pearson correlation coefficient or the Temporal Complementarity Index (TCI) provide valuable information on the phase shift and temporal coordination between renewable sources, they do not account for the relative magnitude of energy production or the actual contribution of each source to the system as is the case in the studies conducted in (Aza *et al.* 2018; Ren *et al.* 2023). Consequently, a high temporal complementarity does not necessarily imply a relevant energy and economic hybrid system, particularly in low-resource environments where one source may be highly complementary but marginal in terms of energy yield.

In this context, neither the Capacity Factor (CF) focused solely on annual wind productivity, nor the Temporal Complementarity Index (TCI) centered on hourly synergy with solar PV can, when taken individually, optimally guide the selection of a wind turbine for efficient hybridization. To address this limitation, this study introduces a novel and original indicator: the Weighted Index of Complementarity and Productivity (WICP). The WICP is specifically designed to evaluate the relevance of wind-solar hybridization and to

support decision-making in the optimal sizing of hybrid photovoltaic–wind systems with battery storage. This innovative criterion coherently combines two fundamental aspects of wind integration:

- Its relative annual productivity, represented by the wind turbine's capacity factor (CF), and
- Its temporal complementarity with photovoltaic generation, represented by TCI.

The WICP, defined in Equation (22), is constructed as a weighted average of the CF and the TCI.

$$WICP = (\alpha * CF + \beta * TCI) * 100 \quad (22)$$

Where: CF is the capacity factor of the wind turbine (typically ranging from 0.2 to 0.5 for viable sites), TCI is the temporal complementarity index with PV generation (usually between 0.5 and 1 in case of good synergy). α and β are weighting coefficients such that α+β=1. These coefficients adjust the relative importance of productivity and complementarity according to project goals. For instance :

- α=β=0.5 reflects a balanced weighting,
- While a choice like α=0.4 and β=0.6, as adopted in this study, favors complementarity, with the aim of reducing storage requirements and avoiding costly oversizing. Indeed, some studies clearly indicate that complementarity is essential for reducing storage requirements and improving system reliability, even when it is not explicitly formalized as a metric (Heide *et al.* 2010; Solomon A. A *et al.* 2020). For example, Heide *et al.* (2010) analyzed the variability of power generation and storage requirements and showed that a solar–wind mix of approximately 40–60 % minimizes generation variability and storage needs, with an 80 % reduction in variability compared to a wind-only system and about a 50 % reduction in storage energy demand compared to mono-source systems.

The WICP varies between 0% and 100%. A WICP value above 40% is considered satisfactory, as it ensures both a minimum acceptable wind production and a significant level of complementarity with solar PV. This threshold is directly derived from commonly accepted minimum performance criteria (CF ≥ 20 % and TCI ≥ 50 %) and provides a design-oriented decision rule for hybrid system selection. In this study, the WICP is used as a preliminary screening indicator to assess the technical relevance of wind energy integration, rather than as a direct optimization parameter. Its role is to discriminate, at the site level, whether hybrid PV/Wind configurations should be further evaluated from a techno-economic perspective. The WICP has proven especially effective in filtering the most suitable wind turbine configurations, in terms of installation height and rated power, for integration into a hybrid PV/Wind energy system with storage. When the WICP remains below the minimum threshold for all turbine configurations, wind-based and hybrid systems are excluded from the optimization stage, and the LCOE analysis is therefore carried out exclusively for PV–battery systems.

2.4.4. Technical Reliability Criterion

The Loss of Power Supply Probability (LPSP) represents the proportion of the annual energy demand that is not met and thus serves as a measure of supply failure probability (Mehallou et al 2025). It is used in our approach to assess the technical reliability of the stand-alone PV/Wind system with battery storage. The LPSP, defined by Equation (23), quantifies the share of unsatisfied energy demand over the total annual energy demand:

.

$$LPSP = \frac{\sum_{t=1}^{8760}\left(\frac{P_{CH}(t)*\Delta t}{\eta_{DC-AC}} - P_{PROD}(t)*\Delta t - (SOC(t-1) - SOC_{\text{MIN}})*\eta_{BAT}\right)}{\sum_{t=1}^{8760} P_{CH}(t)*\Delta t} \quad (23)$$

Where: $P_{PROD}(t)$ is ths Power supplied at time t by the generation (sources) as defined in equation (24),

$$P_{PROD}(t) = (P_{PV}(t) * \eta_{DC-DC} + P_{WT}(t) * \eta_{AC-DC}) \quad (24)$$

$P_{CH}(t)$ is Power demanded by the user at time t.

An LPSP of 10% indicates that 90% of the energy demand is satisfied.

2.4.5. Economic Criterion

The Levelized Cost of Energy (LCOE) is a widely used indicator to evaluate the cost per kilowatt-hour (kWh) produced by a system and to assess the economic affordability of electricity generation systems (Mehallou et al 2025). In this study, the LCOE is expressed by Equation (25):

$$LCOE = \frac{NPV}{\sum_{t=1}^{8760}(P_{PROD}(t))*\Delta t} * CRF \quad (25)$$

Where NPV is the Net Present Value of all costs over the system's lifetime, defined in Equation (26), which accounts for the initial total investment cost C_{IT}, the operation and maintenance costs C_{OM}, assumed to be a fraction m of the investment cost, and the replacement costs $C_R$of the components over the system's lifetime respectively given by equations (27), (28) et (29).

$$NPV = C_{IT} + C_{OM} + C_R \quad (26)$$

$$C_{IT} = C_{Smod} * P_{P_{INST}} + C_{SWT} * P_{WTR_{INST}} + C_{SBAT} * S_{BAT_{INST}} + C_{CONVERT} + C_{SUP-INST-TRANS} \quad (27)$$

$$C_{OM} = C_{IT} * m * F_a \quad (28)$$

$$C_R = \sum_j C_{(IT)_j} * F_{a_j} \quad (29)$$

$P_{P_{INST}}$, $P_{WTR_{INST}}$ and $S_{BAT_{INST}}$ are the optimal installed capacities of the PV generator (in Wp), wind generator (in W), and battery storage (in Wh), respectively. C_{Smod}, $C_{SWT}$and C_{SBAT} are the specific costs of PV modules (EURO/Wp), wind turbines (EURO/W), and batteries (EURO/Wh), respectively. Each specific cost is obtained by dividing the unit market price of the corresponding component by its rated capacity (peak power for PV modules and wind turbines, and nominal energy capacity for batteries). $C_{CONVERT}$ is the total cost of converters (AC/DC, DC/DC, DC/AC), $C_{SUP-INST-TRANS}$ Cost of support structures, transport, and system installation, assumed to be 40% of the total equipment cost (modules, batteries, converters). CRF, F_a and F_{a_j} are the annualization factor, operation & maintenance cost discount factor, and component replacement cost discount factor given by Equations (30), (31), and (32), respectively (Mehallou et al. 2025).

$$CRF = \frac{a_r(1-a_r)^d}{(1+a_r)^d - 1} \quad (30)$$

$$F_a = \begin{cases} \left(\frac{1+i}{a_r - i}\right) * \left[1 - \left(\frac{1+i}{1+a_r}\right)^d\right] & \text{for } a_r \neq i \\ d & \text{for } a_r = i \end{cases} \quad (31)$$

$$F_{a_j} = \sum_{k=1}^{N_{R_j}} \left(\frac{1+i}{1+a_r}\right)^{\frac{k}{N_{R_j}+1}} \quad (32)$$

Where: d System lifetime (years), a_r Real interest rate, i Inflation rate, N_{R_j} Number of replacements of component j during the system's lifetime.

The number of replacements of component j is calculated using Equation (33):

$$N_{R_j} = \left(\frac{d}{D_j}\right) - 1 \quad (33)$$

Where $D_j$is the lifetime (in years) of component j.

2.5. Optimization problem

Based on the mathematical models of the system components, the performance indicators, and the battery aging model, the optimal sizing problem is formulated as the system of equations presented in (34). The objective is to determine the peak power of the photovoltaic (PV) generator and/or the rated power of the wind turbine ($P_P$and/or P_{WTR}), as well as the storage autonomy duration (N_H) in hours, that can maximize the energy supply to the user while minimizing the cost. The system must satisfy a technical reliability constraint: the Loss of Power Supply Probability (LPSP) must not exceed a user-defined threshold ($LPSP_{MAX}$, in %). At the same time, the state of charge of the battery bank ($SOC(t)$, in Wh) must remain within two bounds, namely the minimum state of charge SOC_{MIN} and the maximum state of charge SOC_{MAX}, as defined by Equations (35) and (36).

$$\boldsymbol{S};\begin{cases} Min\ LCOE\ (P_P, P_{WTR}, N_H) \\ LPSP(P_P, P_{WTR}, N_H) \leq LPSP_{MAX} \\ SOC_{MIN} \leq SOC(t) \leq SOC_{MAX} \\ P_{P_{MIN}} \leq P_P \leq P_{P_{MAX}} \\ P_{WTR_{MIN}} \leq P_{WTR} \leq P_{WTR_{MAX}} \\ 1 \leq N_H \leq N_{H_{MAX}} \end{cases} \quad (34)$$

$$SOC_{MAX} = \mu * S_{BAT} * U_{BAT} \quad (35)$$

$$SOC_{MIN} = (1 - DOD_{MAX})SOC_{MAX} \quad (36)$$

Where; S_{BAT} and U_{BAT} are the adjusted storage capacity (in Ah) and the battery bank voltage (in V), respectively, μ: a percentage term representing the maximum energy level not to be exceeded in the battery during charging. For example, if μ =90% this means the battery should not be charged beyond 90% of its nominal capacity, DOD_{MAX}: the maximum depth of discharge of the battery, expressed in percentage.

The power ranges for both PV and wind generators are defined by Equations (39), (40), (41), and (42), based on the user's daily load using standard sizing formulas given by Equations (37) and (38) (Konate 2025)**.** In addition, statistical analysis of the meteorological data (solar irradiance and wind speed) and component performance assumptions was carried out to define realistic power ranges. This helps to guide the techno-economic optimization process and reduce unnecessary search space.

$$P_P = \frac{E_D * G_{ref}}{I_D * \eta_g} \text{ (Classical PV sizing equation)} \quad (37)$$

$$P_{WTR} = \frac{E_J}{E_{SJ} * \eta_W} \text{ (Classical wind sizing equation)} \quad (38)$$

$$P_{P_{MIN}} = \frac{E_D * G_{ref}}{I_{D_{MAX}} * 0.85} \text{ (Most favorable PV scenario)} \quad (39)$$

$$P_{P_{MAX}} = \frac{E_D * G_{ref}}{I_{D_{MIN}} * 0.6} \text{ (Most unfavorable PV scenario)} \quad (40)$$

$$P_{WTR_{MIN}} = \frac{E_D}{E_{SD_{MAX}} * 0.9} \text{ (Most favorable wind scenario)} \quad (41)$$

$$P_{WTR_{MAX}} = \frac{E_D}{E_{SD_{MIN}} * 0.9} \text{ (Most unfavorable wind scenario)} \quad (42)$$

Where: E_D is the user's daily energy demand (kWh/day),G_{ref} is the reference irradiance (typically 1 kW/m²)I_D is the average daily irradiation on a tilted surface (kWh/m²/day), $\eta_g$is the overall efficiency of the PV system (typically between 0.60 and 0.85), E_{SD} is the specific daily energy produced by 1 kW wind turbine (kWh/kW/day), η_W is the overall efficiency of the wind system (typically 0.90), $I_{D_{MIN}}$, $I_{D_{MAX}}$, $E_{SD_{MIN}}$ and $E_{SD_{MAX}}$ are the minimum and maximum values, respectively, of the average daily irradiation and specific daily energy produced by 1 kW of wind turbine, extracted over the 365 days of the year. These are defined for each day using Equations (43) and (44):

$$E_{SD} = \sum_{t=1}^{24} (P_{WT}(t)/1000) \text{ (in kWh/kW/day)} \quad (43)$$

$$I_D = \sum_{t=1}^{24} (G_I(t)/1000) \text{ (inkWh/m²/day)} \quad (44)$$

For series/parallel arrangements of system components (PV modules, batteries, wind turbines), the formulas used are provided in Appendix A.

2.6. Proposed iteratives resolution algorithms

Figure 3 illustrates the general flowchart of the proposed optimal sizing program. After entering the various input parameters of the model (time series of meteorological data, unit technical characteristics of components, unit costs, installation site altitude and module tilt), the Capacity Factor (CF) of an onshore micro-wind turbine of any nominal power is evaluated to determine the most suitable system type for the location.

- If the capacity factor is less than 20%, the site is not viable for wind turbine installation. Therefore, the appropriate facility for the site is the standalone PV-Battery system (SYST_PV_BAT). In this case, the program proceeds, and the ALGO_PV_BAT algorithm (whose flowchart is presented in Figure B1, Appendix B) is executed to deliver the OPTIMAL SOLUTION A, which offers the best compromise between LPSP and LCOE.
- If the capacity factor is greater than or equal to 20%, the Weighted Index of Complementarity and Productivity (WICP) is calculated to assess the relevance of hybridization between solar and wind sources.
    - If WICP < 40%, hybridization is not beneficial. In this case, the individual systems SYST_PV_BAT and SYST_EOL_BAT are both suitable for the site, but they do not necessarily yield the same cost per kWh. The designer must determine the best compromise between

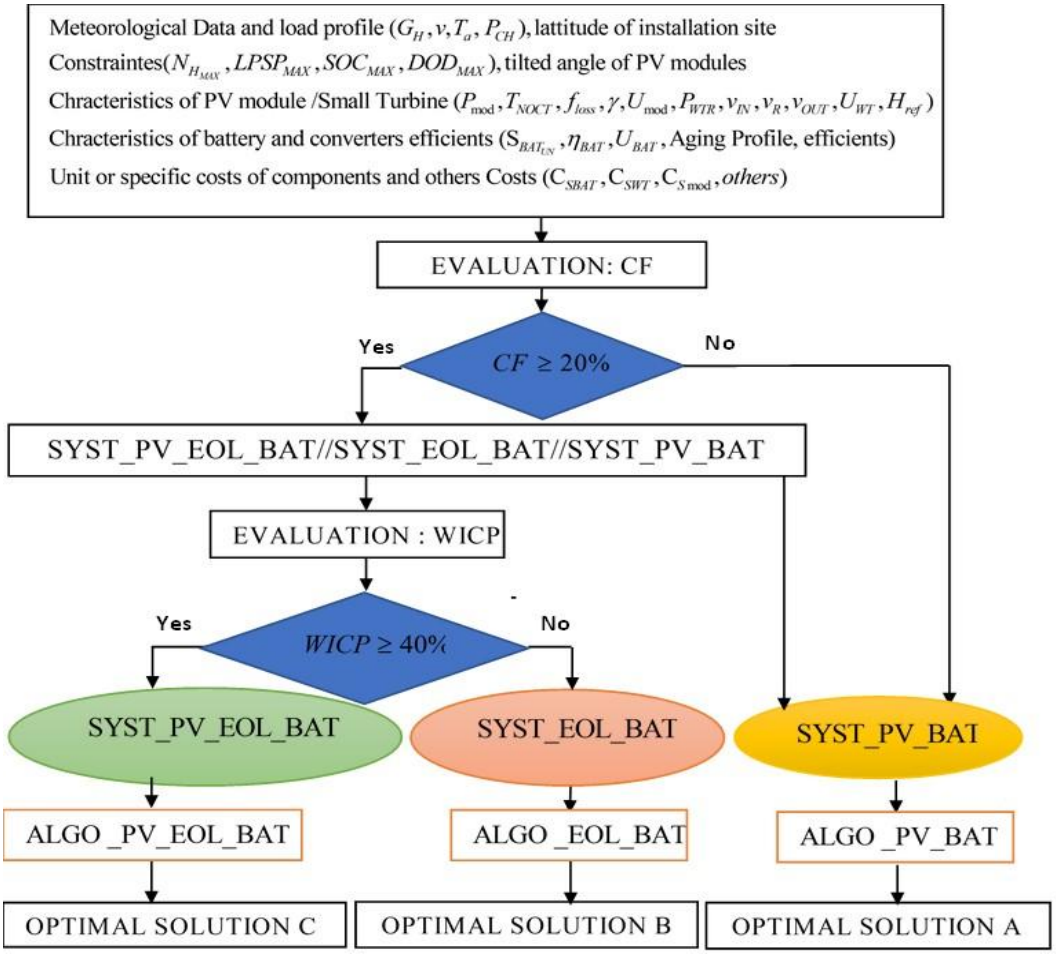

Fig 3. General flowchart of the optimal sizing program for a standalone PV/Wind system with battery storage

LPSP and LCOE for each system. To do this, they must first execute the instructions in ALGO_EOL_BAT (flowchart shown in Figure B2, Appendix B), then execute ALGO_PV_BAT, and finally select the most cost-effective system for the user (OPTIMAL SOLUTION B or OPTIMAL SOLUTION A).

- If WICP ≥ 40%, hybridization between solar and wind becomes attractive. In this case, the systems SYST_PV_BAT and SYST_PV_EOL_BAT are both suitable, though they may not yield the same LCOE. Again, the designer must evaluate the best trade-off between LPSP and LCOE. First, the instructions in ALGO_PV_EOL_BAT are executed (flowchart in Figure B3, Appendix B), followed by ALGO_PV_BAT, to choose the most economical system for the user (OPTIMAL SOLUTION C or OPTIMAL SOLUTION A)

3. Case study: Nagreongo site

To implement the sizing methodology proposed in this study, the rural site of Nagréongo, located at about 35 km east of Ouagadougou (Burkina Faso), was selected as the application site. Like many rural localities in sub-Saharan Africa, access to reliable electricity in this area remains limited, and decentralized renewable energy systems represent a promising solution for electrification. The site therefore provides a relevant case study for evaluating the technical and economic performance of standalone renewable energy systems with battery storage under real climatic and consumption conditions. This locality, situated at latitude 12°24'30'' and longitude 1°11'14'', is equipped with a meteorological station that enables the collection of climatic data. The data used are for the year 2023, they include horizontal solar irradiance (Figure 4a), wind speed measured at 5 meters above ground level (Figure 4b), and ambient temperature (Figure 4c). Their hourly profiles, shown in Figure 4, reveal significant variations throughout the year, reflecting the fluctuating nature of energy resources (solar and wind) as well as temperature. The meteorological profiles shown in Figure 4 highlight the strong temporal variability of the available renewable resources at the Nagréongo site. The solar irradiance profile exhibits the typical diurnal cycle with high daytime values frequently approaching 1000 W/m², indicating a favorable solar potential for photovoltaic energy production. In contrast, wind speeds measured at 5 m above ground remain generally low and highly irregular throughout the year, suggesting limited wind energy potential at the site. Finally, the ambient temperature varies between approximately 18 °C and 40 °C, which may influence both the performance of PV modules and the aging behavior of batteries. These characteristics are therefore important parameters to consider in the sizing and techno-economic optimization of the energy system. In order to analyze the impact of the consumption profile on the optimal system configuration and the LCOE, three

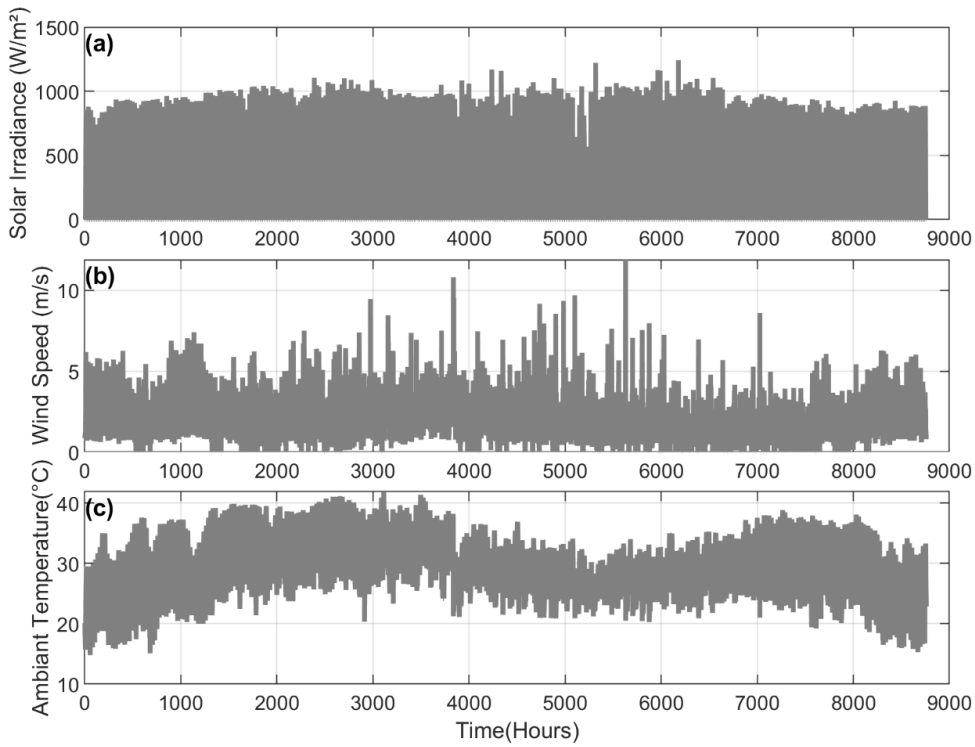

Fig 4. Meteorological data of Nagréongo site a) Hourly profile of horizontal solar irradiance; b) Hourly profile of wind speed measured at 5 m above ground; c) Hourly profile of ambient temperature.

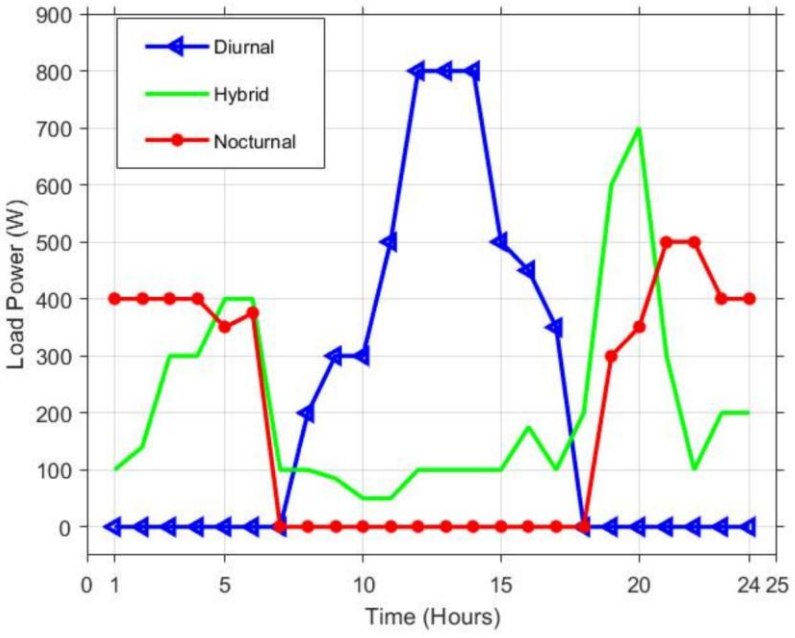

Fig 5. Hourly load profiles of three specific households, each with an identical daily energy demand of 5 kWh, assumed to be in the Nagréongo area.

daily consumption profiles were considered for simulations and presented in Figure 5. Each represents a specific household consumption with an identical energy demand of 5 kWh per day. These profiles, illustrated in Figure 5, differ in their hourly distribution:

- The Diurnal profile corresponds to consumption exclusively during the day, between sunrise and sunset;

- The Nocturnal profile corresponds to consumption only during the night, after sunset;
- The Hybrid profile combines both day and night consumption.

The load profiles presented in Figure 5 represent three different temporal distributions of electricity demand with the same daily energy consumption (5 kWh). The diurnal profile shows a single peak around midday (12:00–14:00 at 800 W), well aligned with PV production, which limits storage needs and improves system performance. In contrast, the nocturnal profile exhibits two peaks (1:00–4:00 at 400 W and 20:00–22:00 at 500 W), occurring outside solar hours, thus increasing reliance on battery storage. The hybrid profile represents an intermediate case, with a morning peak (5:00–6:00, at 400 W) and a higher evening peak (19:00–20:00 at 700 W), leading to a balanced use of direct PV supply and storage. These differences highlight that the timing and magnitude of demand peaks strongly influence system sizing, storage requirements, and the resulting LCOE as it demonstrated in results section (section 4.8).

In this study, it is assumed that each profile remains the same every day of the year. The technical and economic characteristics of the system components, as well as their lifetime, are presented in Table C1 in Appendix C. The interest and inflation rates used are 8% and 3% respectively, in line with the assumptions made in (Yamegueu, Nelson and Boly 2024) for the LCOE calculation. The PV modules used are 265 Wp modules. They are oriented due south and tilted at 12°, which corresponds to the latitude of Nagréongo. Table C2 in Appendix C presents the technical specifications of the onshore micro-wind turbines (ranging from 0.2 to 1 kW) used in the study. These turbines represent small-scale wind technologies typically considered for decentralized rural electrification systems. Their rated powers and cut-in wind speeds are compatible with low-power standalone applications, allowing the evaluation of different turbine configurations under the wind conditions observed at the Nagréongo site. The number of battery cycles as a function of depth of discharge, for a specific usage (regular cycling) at the reference temperature (25 °C), provided by the manufacturers represented in Figure 7a. These data are used to predict the Battery life time at the Nagreongo site average ambient temperature(28.92°C). Finally, Table C3 presented in Appendix C summarizes the technical constraints used in the optimization process. These constraints are defined to ensure realistic system operation while balancing reliability, economic performance, and component lifetime. The LPSP values (0%, 5%, and 10%) represent different reliability levels commonly adopted in off-grid systems. Battery limits (DOD = 80% and SOC = 90%) follow manufacturer recommendations to reduce degradation and extend lifetime. A maximum autonomy of 72 hours is considered to ensure system resilience under low renewable resource conditions. Finally, the PV (265 Wc) and wind (200 W) sizing steps are based on commercially available component ratings, ensuring practical and implementable system configurations.

4. Result and Discussion

4.1. Influence of installation height on Weibull parameters and annual average wind speed

Figure 6a) illustrates the influence of altitude or installation height on the Weibull parameters and the annual average wind speed. It can be observed that between 5 m and 80 m in height, both the annual average wind speed and the Weibull scale factor indicators of wind resource quality increase slightly, remaining close to each other and ranging between 2 m/s and 3.4 m/s. However, the Weibull shape factor remains constant at 1.53 regardless of the height. These low values of annual average wind speed and scale factor clearly indicate that the Nagréongo site has very limited wind potential. Similar wind resource characteristics with low mean wind speeds and Weibull parameters have been reported for several inland West African sites (Ahmed, Bello and Habou 2013; Olomiyesan *et al.,* 2017). The invariance of the Weibull shape parameter k with height indicates that the statistical distribution of wind speeds remains unchanged throughout the atmospheric layer considered. This suggests a stable wind regime dominated by persistent low-speed conditions, with limited occurrence of high-speed events. Such behavior is typical of inland Sahelian sites characterized by high surface roughness and weak vertical wind shear.

4.2. Influence of installation height and Wind Rated Power on the Wind Capacity Factor (CF) and on the Weighted Index of Complementarity and Productivity (WICP)

Figure 6b) shows the variation of the capacity factor (CF) of wind turbines as a function of installation height and Wind rated power. It can be observed that the CF increases with height for a given power rating but remains nearly unchanged when the rated power varies at a constant height. Regardless of the height (between 5 m and 80 m) or rated power (from 0.2 kW to 1 kW) considered, the capacity factor remains less than or equal to 11%. This low performance is due to the relatively low annual average wind speed and scale factor observed at the site, as illustrated in Figure 6a). The weak sensitivity of the capacity factor to the rated power highlights a structural limitation of wind exploitation at this site. Since the wind speed rarely reaches the rated wind speed of the turbines of 10m/s mentioned in table 2, increasing the nominal power does not translate into higher energy yield. Instead, turbines operate predominantly in partial-load conditions, leading to similarly low capacity factors across all rated powers. Since the CF is well below the minimum threshold of 20% required to consider a viable wind installation, the Nagréongo site is not suitable for wind energy exploitation, regardless of the turbine size (small or large). Such low capacity factors generally indicate limited economic viability of wind installations, particularly for small-scale turbines (Ohunakin, Oyewola and Adaramola 2013). Under these conditions, a standalone photovoltaic system with battery storage appears to be a more suitable solution, considering the good solar potential of the site, estimated at around 5.5 kWh/m²/day. Consequently, in the developed MATLAB program (whose general flowchart is presented in Figure 3), only the section dedicated to the PV_BAT algorithm (Figure B1, Appendix B) will be running to determine the optimal configuration of the PV system with storage for the user. Figure 6c) illustrates the evolution of the Weighted Index of Complementarity and Productivity (WICP) as a function of installation height and the rated power of micro-wind turbines. Unlike the Capacity Factor (CF), the WICP slightly decreases with increasing altitude for a given power, but remains generally constant regardless of the rated power at a given height. For all heights between 5 m and 80 m, as well as for all rated powers ranging from 0.2 kW to 1 kW, the WICP does not exceed 25.8%. This value remains well below the minimum threshold of 40% required to ensure an acceptable balance between productivity and complementarity. These low WICP values indicate that wind generation does not effectively compensate for periods of low solar availability. This suggests a strong temporal correlation between low wind speeds and low solar resource

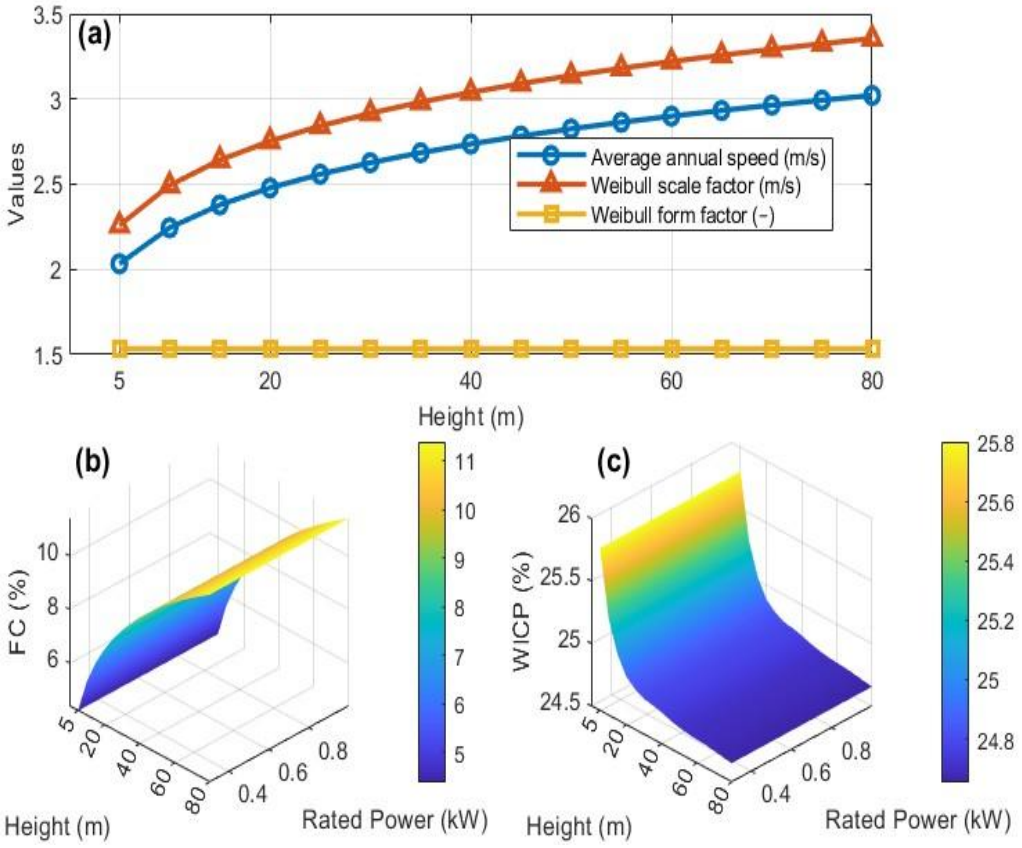

Fig 6. Wind resource assessment and performance indicators as a function of hub height and rated wind turbine power : (a) variation of the annual average wind speed, Weibull scale parameter, and Weibull shape parameter with hub height; (b) evolution of the Wind capacity factor (CF, %) as a function of hub height and rated wind turbine power ; (c) variation of the Wind weighed index of complementarity and productivity (WICP, %) as a function of hub height and rated wind turbine power.

periods, particularly during calm atmospheric conditions. As a result, wind energy fails to play a meaningful balancing role in the hybrid system, regardless of installation height or turbine size.

This reflects both the low productivity of the Aeolos micro-wind turbines considered and their poor complementarity with solar energy, regardless of installation height. These results also confirm the non-viability of the Nagréongo site for wind energy system, as already indicated by the CF analysis presented in Figure 6b). Overall, Figure 6 demonstrates that increasing installation height alone cannot overcome the intrinsic limitations of the wind resource at the Nagréongo site. Even when considering higher towers and different turbine ratings, both the energy productivity and the complementarity with solar energy remain insufficient. These results justify the exclusion of wind energy from the final sizing stage and confirm the relevance of a PV–battery-only configuration for this site. It should be noted that the WICP is used exclusively as a preliminary indicator for assessing the technical relevance of hybridization. When its value remains below the minimum viability threshold, as in the present case, wind-based configurations are excluded from further techno-economic optimization.

4.3. Correction of Nominal Aging and Storage Capacity at Ta_{moy}

Figure 7a) shows the cycling aging curves of the Lithium SuperPack batteries used in this study. One at the reference temperature (25 °C) and the other at the site's average ambient temperature (28.92 °C). The 25 °C curve was plotted based on the manufacturer's data, while the 28.92 °C curve results from applying a thermal correction coefficient specific to the battery technology used, in order to account for the impact of temperature on aging. This correction approach allows the manufacturer-provided aging data, usually given under standard laboratory conditions, to be realistically adapted to the actual climatic conditions of the installation site. By integrating the site-average ambient temperature into the aging model, the proposed methodology improves the representativeness of the battery lifetime estimation under real operating conditions. It is clearly observed that the curve at 25 °C lies above the one at 28.92 °C, indicating that a temperature higher than the reference significantly reduces battery lifespan by decreasing the number of supported cycles. For instance, at a depth of discharge (DOD) of 80%, the number of cycles decreases from approximately 2500 cycles at 25 °C to about 1900 cycles at 28.92 °C, corresponding to a reduction of nearly 24%. This degradation can be attributed to accelerated electrochemical reactions and increased internal resistance at elevated temperatures, which intensify aging mechanisms such as electrolyte decomposition and electrode material degradation. Similar observations have been reported in recent studies showing that high operating temperatures accelerate lithium-ion battery degradation through mechanisms such as electrolyte decomposition and electrode material deterioration (Leng, Tan and Pecht 2015; Shen *et al.*, 2025). Such a reduction in cycle life has direct implications for system sizing and economic

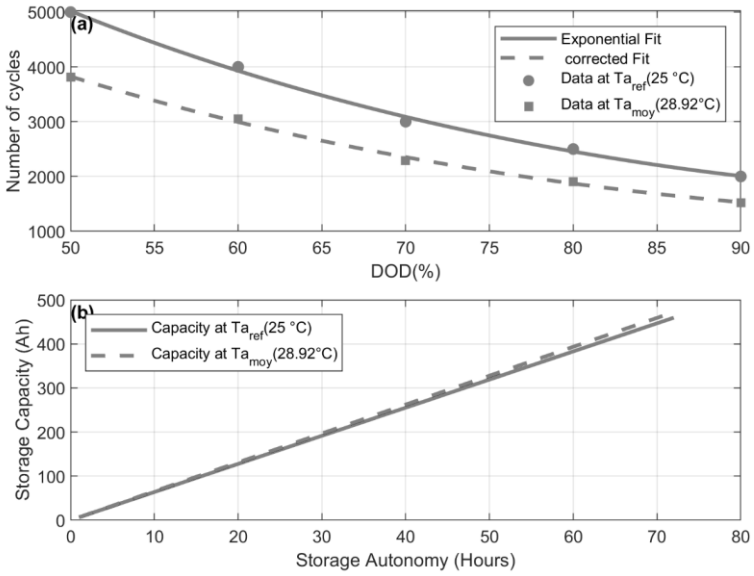

Fig 7. Corrected Storage Capacity and Cycle Aging under Reference and Ambient Temperature. a) Regular cycling aging of the storage at reference temperature Ta_{ref} and average ambient temperature Ta_{moy}. b) Evolution of storage capacity as a function of autonomy duration at Ta_{ref} and at Ta_{moy}

performance. Neglecting the temperature effect would lead to an overestimation of battery lifetime and, consequently, an underestimation of replacement costs over the project lifetime, which may result in suboptimal or economically unrealistic system configurations. Figure 7b), on the other hand, illustrates the evolution of storage capacity as a function of autonomy duration at these two temperatures. The curves show a linear relationship between capacity and autonomy. Furthermore, the 25 °C curve is slightly below that of 28.92 °C, suggesting that in this case, a temperature slightly higher than the reference has only a minimal impact on the nominal storage capacity. This slight increase in apparent capacity at higher temperature is mainly due to improved electrochemical kinetics, which temporarily enhance charge transfer processes. However, this short-term gain in usable capacity does not compensate for the long-term acceleration of aging observed in Figure 7a). Consequently, while the impact of temperature on nominal storage capacity remains marginal, its effect on cycling aging is

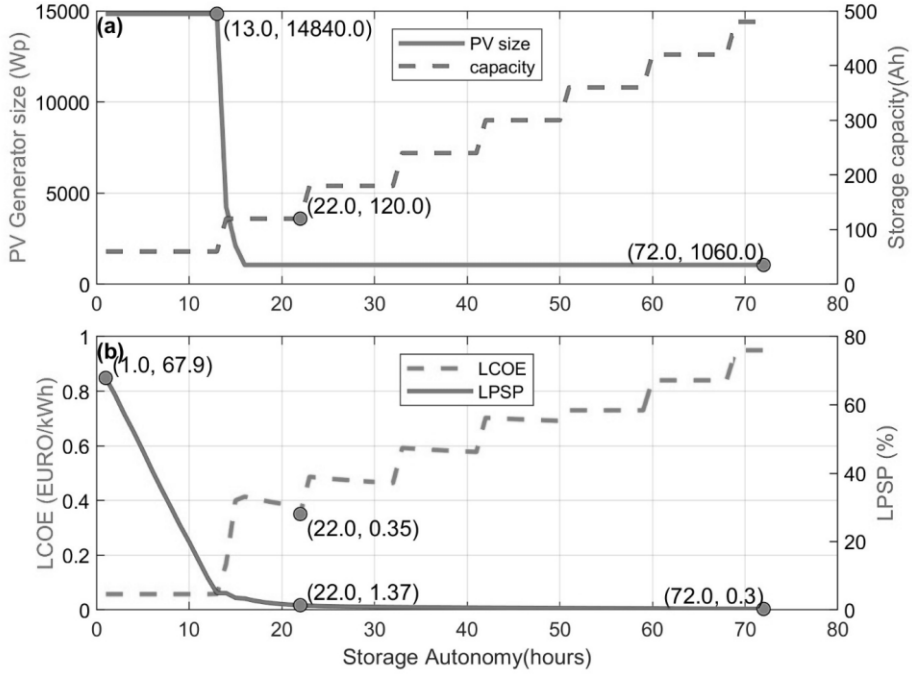

Fig 8. Influence of Storage Autonomy on System Sizing and Performance Indicators under a maximum LPSP set at 5%, a real operating temperature of 28.92°Cand for the hybrid consumption profile: a) Evolution of PV generator size, storage capacity as a function of storage autonomy and b) Evolution of LPSP, and LCOE as a function of storage autonomy

substantial. This highlights the importance of prioritizing aging correction over capacity correction when modeling battery behavior in hot climates such as the study site. Overall, these results confirm that integrating temperature-dependent aging models is essential for achieving realistic battery lifetime prediction and robust techno-economic optimization of standalone PV systems operating under real environmental conditions.

4.4. Optimal configuration of the PV_BAT system for the Hybrid consumption profile.

Figures 8 a) and b) show the evolution of the photovoltaic generator size, storage capacity, LPSP, and LCOE as functions of storage autonomy, for a maximum LPSP set at 5% and a hybrid consumption profile under a real operating temperature of 28.92°C. When the autonomy ranges from 1 to 13 hours, the PV generator size, storage capacity, and LCOE remain constant at 14,840 Wp (upper limit of the search space), 60 Ah (unit battery capacity), and 0.058 EURO/kWh, respectively. During this period, the LPSP decreases linearly, from over 60% to 5.02%. This indicates that for autonomy less than or equal to 13 hours, even if the LCOE is minimal, no configuration can meet the 5% LPSP threshold due to insufficient storage capacity. Between 13 h and 16 h of autonomy, the PV generator size drops sharply from 14,840 Wp to 1,060 Wp, then remains constant beyond this point. Over the same range, the LPSP decreases from 5.02% to 3.40%, before continuing to decline slightly beyond 16 h. In parallel, the LCOE increases sharply from 0.058 EURO/kWh to 0.40 EURO/kWh, then decreases between 16 h and 22 h to reach 0.35 EURO/kWh, before gradually increasing again in steps beyond 22 h. These results show that increasing autonomy beyond 16 hours only marginally reduces the LPSP but significantly increases the LCOE. Thus, any configuration offering at least 16 hours of autonomy can be considered technically reliable. Among these, the configuration corresponding to 22 hours of autonomy is the most cost-effective, with the lowest LCOE. This optimal configuration, which satisfies at least 95% of the annual energy needs of a household with a hybrid consumption profile, requires a PV power of 1,060 Wp and a minimum storage capacity of 120 Ah. It corresponds to an arrangement composed of one string of four 12 V/265 Wp PV modules and two strings of four 12 V/60 Ah batteries.

4.5. Influence of Storage Autonomy and operating temperature on Battery Lifetime, Number of Storage Replacements and levelized cost of energy (LCOE) for the Hybrid Load Profile

Figures 9 illustrate the combined influence of storage autonomy and operating temperature on storage lifetime, the number of battery replacements over a 20-year project horizon, and the levelized cost of energy (LCOE), under two thermal conditions: a reference temperature of 25 °C and the site's average ambient temperature of 28.92 °C. Figure 9 a) shows that storage lifetime increases with autonomy, regardless of operating temperature. Higher autonomy results in lower average depths of discharge (DoD), thereby reducing cyclic stress and extending battery lifetime. This trend is well documented in recent studies on electrochemical energy storage systems, which emphasize the dominant role of DoD in cyclic degradation mechanisms (Andrenacci et al., 2021; Kim and Shin, 2023). However, temperature has a clearly detrimental effect. For autonomies below 15 h, storage lifetime decreases from about 8.3 years at 25 °C to 6.3 years at 28.92 °C, while for autonomies of 22 h and 51 h it decreases from 13.5 and 26.6 years to 10.3 and 20.2 years, respectively. Overall, this corresponds to an average lifetime reduction of about 24%

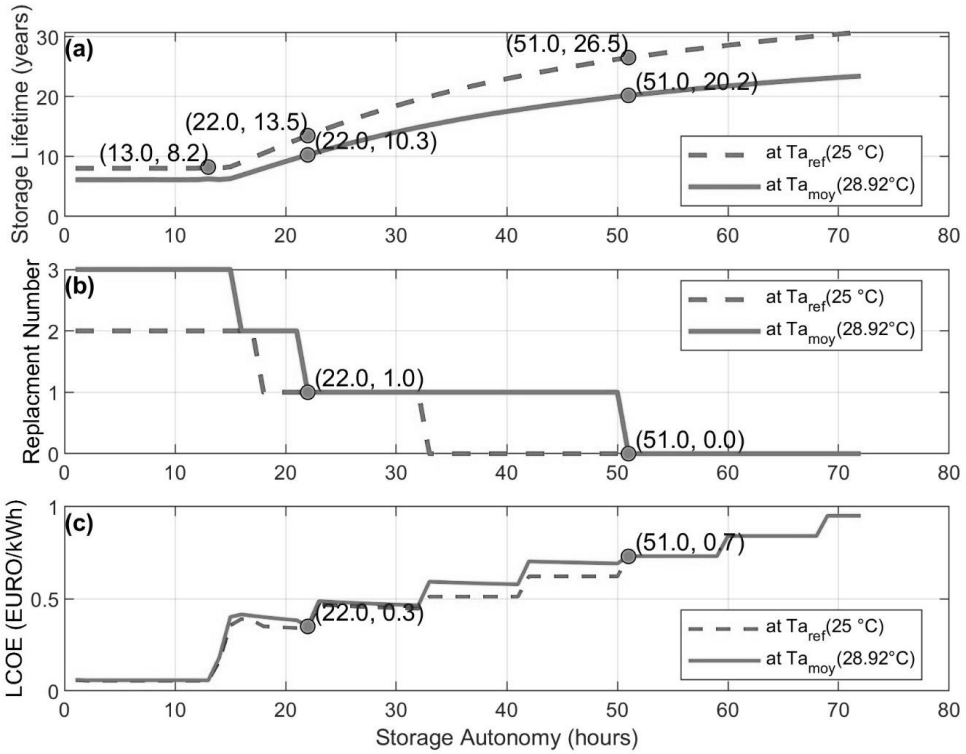

Fig 9. Impact of Storage Autonomy and operating temperature on Battery Lifetime, Replacement Frequency and LCOE under a 5% LPSP Constraint for the Hybrid Load Profile. **a)** Evolution of battery lifetime with increasing storage autonomy at 25°C and at 28.92°C. **b)** Evolution of the number of battery replacements with storage autonomy at 25°C and at 28.92°C. c) Evolution of LCOE with increasing storage autonomy at 25°C and at 28.92°C.

when temperature increases from 25 °C to 28.92 °C, consistent with aging-aware models showing accelerated degradation at elevated temperatures (Leng et al., 2015; Du et al., 2024; Madani et al., 2025).

Figure 9 b) reflects these trends in terms of replacement frequency. At low autonomies (<15 h), the number of replacements is maximal, reaching up to three at 28.92 °C and two at 25 °C. However, the impact of temperature on replacement frequency is governed by threshold effects related to the finite project lifetime. In the autonomy ranges of 16–17 h and 22–32 h, the temperature-induced reduction in lifetime is insufficient to trigger an additional replacement over 20 years, leading to the same number of replacements under both thermal conditions despite different lifetimes. Beyond about 30 h at 25 °C and 50 h at 28.92 °C, no replacement is required, indicating that higher temperatures increase the minimum autonomy needed to avoid battery renewal and thus impose an additional sizing constraint.

Figure 9 c) highlights a clear techno-economic trade-off. The LCOE generally increases with autonomy due to higher investment costs associated with larger storage capacities, while its stepwise variations are directly linked to changes in the number of replacements. For low autonomies (1–13 h), the LCOE remains nearly identical at both temperatures, as the marginal cost of an additional replacement at 28.92 °C is outweighed by the small installed capacity and the dominance of initial system costs. Similarly, in the autonomy ranges of 16–17 h and 22–32 h, the LCOE is weakly affected by temperature since replacement-related costs remain unchanged. In contrast, for autonomies between 33 h and 50 h, the LCOE is systematically higher at 28.92 °C, with a maximum increase of about 12%, due to reduced battery lifetime and additional replacement cycles, in line with previous studies (Gbadegesin et al., 2019; Brihma Fouzia, 2023; Witharama et al., 2024). At very high autonomies (>50 h), the LCOE increase is mainly driven by the stepwise growth of installed storage capacity rather than by replacement effects.

Overall, Figure 9 demonstrates that storage autonomy and operating temperature are strongly coupled parameters. While higher temperatures systematically accelerate battery aging, their impact on replacement frequency and LCOE is discontinuous and governed by replacement thresholds. Increasing autonomy mitigates both cyclic and thermal aging but at the expense of higher capital costs, revealing a fundamental techno-economic trade-off. Neglecting temperature effects may therefore lead to an overestimation of storage lifetime and, depending on the autonomy range, an underestimation of the LCOE, particularly in hot climates. For the optimal PV configuration identified in Figure 8 (22 h autonomy and 120 Ah capacity), the storage lifetime is estimated at 10.3 years at 28.92 °C, resulting in a single battery replacement over the 20-year project lifetime.

4.6. PV Generator Production, Battery State of Charge, and Number of Cycles Counted Using the Rainflow Method for the Hybrid Consumption Profile under a real operating temperature of 28.92°C

Figures 10 a) and b) respectively show the hourly evolution of the power delivered by the photovoltaic generator and the battery state of charge, for the real optimal configuration of the PV_BAT system corresponding to the hybrid consumption profile, with a maximum LPSP set at 5%.This configuration reflects real operating conditions, including the actual ambient temperature of 28.92 °C and the variability of solar resource and load demand over an entire year, ensuring that both production

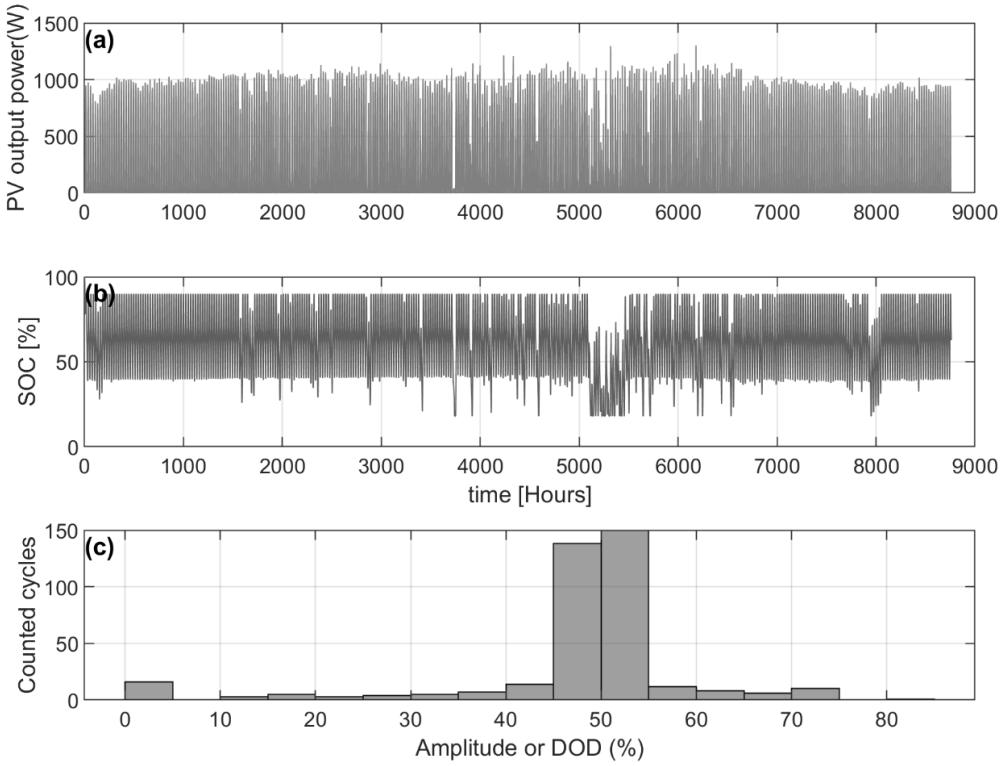

Fig 10. PV Generator Output, Storage Behavior, and Cycle Counting for the Optimal PV-Battery System (Hybrid Load, LPSP ≤ 5%) under a real operating temperature of 28.92°C. a) Hourly variation of PV generator power output; b) Hourly evolution of battery state of charge (SOC); c) Number of cycles or micro-cycles identified by the Rainflow cycle counting algorithm.

and storage dynamics are realistically captured. A strong correlation is observed between the battery state of charge and the power output of the PV generator: low charge levels coincide with low solar production, and vice versa. During periods of high photovoltaic production, the battery is progressively recharged, leading to an increase in the state of charge, whereas extended periods of low or intermittent solar generation result in deeper battery discharge to meet the load demand. This behavior confirms the central role of the battery in compensating for the intermittency of the photovoltaic source under hybrid consumption conditions. It can also be observed that the state of charge remains within the predefined operational limits for most of the year, indicating that the selected PV and battery capacities are well balanced. The occasional deep discharges correspond to critical periods of low solar availability and high demand, yet the imposed LPSP constraint of 5% is still respected. Figure 10 c) presents the number of charge/discharge cycles identified by the Rainflow algorithm based on the state of charge profile shown in Figure 10 b). The Rainflow counting method allows complex and irregular state-of-charge variations to be decomposed into equivalent charge/discharge cycles, characterized by their depth-of-discharge amplitude, which is essential for an accurate evaluation of cycling-induced battery aging. A total of 382 cycles were counted, most of which exhibit depth-of-discharge amplitudes between 45% and 55%. The dominance of medium-amplitude cycles indicates that the battery predominantly operates around moderate depth-of-discharge levels, which is generally favorable for lithium-based battery lifetime compared to frequent deep cycling. When combined with the temperature-corrected aging model introduced in the previous section, these cycle distributions enable a realistic estimation of battery lifetime under actual climatic conditions, as both cycle amplitude and operating temperature are key drivers of degradation. Overall, this analysis demonstrates that the proposed optimization framework not only ensures acceptable supply reliability but also leads to a battery operating regime that limits excessive aging, thereby contributing to the long-term technical and economic viability of the PV_BAT system under hybrid load conditions.

4.7. Influence of $LPSP_{max}$ on the Real Optimal Configuration and the LCOE

Table 1 highlights the influence of the maximum allowed Loss of Power Supply Probability (LPSPmax) on the real optimal configuration and on the Levelized Cost of Energy (LCOE) of the PV with batteries system (SYST_PV_BAT), for the hybrid consumption profile, assuming a maximum Depth of Discharge (DOD) of 80% and a maximum State of Charge (SOC) of 90% under a real operating temperature of 28.92 °C. The LPSPmax parameter directly reflects the reliability level imposed on the system and plays a key role in the optimization process, as stricter reliability requirements generally lead to higher installed capacities and increased system costs. This behavior is widely reported in the literature, where reducing the LPSP leads to larger system sizing and higher overall costs (Kaabeche, Belhamel and Ibtiouen 2011; Halabi et al., 2017). It can be observed that the system configuration remains unchanged when LPSPmax increases from 5% to 10%. This indicates that, beyond a certain reliability threshold, the available photovoltaic production and storage capacity are already sufficient to accommodate a moderate increase in unmet load without requiring additional system oversizing. However, the associated LCOE values show variations, likely due to differences in annual energy production resulting from the varying LPSP levels. Indeed, a higher LPSP allows a greater fraction of the demand to remain unsupplied during critical periods, which slightly reduces the effective delivered energy and consequently affects the LCOE, even when the installed capacities remain identical. Conversely, when LPSPmax is reduced from 5% to 0%, the PV generator size, storage capacity, autonomy, battery lifetime, and LCOE nearly double. Enforcing a zero-loss criterion (LPSP = 0%) requires the system to withstand the most unfavorable combinations of low solar irradiation and high load demand, which leads to a substantial increase in both generation and storage capacities. These results demonstrate that achieving full coverage of the energy demand (LPSP = 0%) requires a highly oversized system. Although this configuration improves battery lifetime due to reduced cycling stress, the economic penalty associated with the increased investment cost outweighs the benefits under the considered real operating temperature of 28.92 °C. with a significant economic impact. Among the three configurations presented, the one with the lowest LCOE represents the best economic compromise. This configuration therefore represents the most balanced trade-off between system reliability and economic performance, making it the most suitable choice for practical implementation under hybrid consumption conditions. Overall, this analysis highlights the strong sensitivity of system cost and sizing to the imposed reliability level and confirms that moderate LPSP values can lead to economically optimal designs without excessively compromising supply security. Similar trade-offs between reliability and economic performance have been highlighted in previous studies on standalone and hybrid renewable energy systems (Kaabeche, Belhamel and Ibtiouen 2011; Halabi *et al.*, 2017).

4.8. Influence of the Consumption Profile on the Optimal Configuration or the LCOE

Table 2 presents the real optimal configurations of the PV system with batteries (SYST_PV_BAT), obtained using the sizing method proposed in this study. The analysis focuses on three consumption profiles representing three fictitious households located in Nagréongo, each with an identical daily

Table 1
Influence of LPSPmax on the real optimal configuration and LCOE of the SYST_PV_BAT system for the hybrid consumption profile with DODmax = 80% and SOCmax = 90% under a real operating temperature of 28.92 °C

$LPSP_{MAX}$ (%)	PV generator Size (Wp)	Storage Capacity (Ah)	Storage Autonomy (Hours)	Storage Life time (Years)	N_{Hoff} (Hours)	LPSP (%)	LCEO (EURO/kWh)
10	1060	120	22	10.77	0	7.01	0.44
5	1060	120	22	10.20	0	1.37	0.35
0	2120	300	50	20.07	0	0	0.54

Table 2
Influence of the consumption profile on the optimal configuration of the SYST_PV_BAT system for an identical daily energy need of 5 kWh, with DODmax = 80%, LPSPmax = 5%, and SOCmax = 90% under a real operating temperature of 28.92°C

Profile	PV generator Size (Wp)	Storage Capacity (Ah)	Storage Autonomy (Hours)	Storage Life time (Years)	N_{Hoff} (Hours)	LPSP (%)	LCEO (EURO/ kWh)
Diurnal	1060	60	5	13.35	14	1	0.20
Nocturnal	1060	120	11	7.50	12	2.52	0.41
Hybrid	1060	120	22	10.20	0	1.37	0.35

energy demand of 5 kWh. These configurations were determined considering a maximum Depth of Discharge (DOD) of 80%, a maximum Loss of Power Supply Probability (LPSPmax) of 5%, and a maximum State of Charge (SOCmax) of 90%. It is observed that, despite the identical daily demand, the optimal configurations differ depending on the profile. This clearly shows that not only the total daily energy demand but also its temporal distribution plays a critical role in system sizing, as the mismatch between load periods and photovoltaic production hours directly affects storage requirements and system performance. The LCOE of the configuration associated with the nocturnal profile is the highest, followed by that of the hybrid profile because the storage lifetime associated with the nocturnal profile is lowest. These two values are approximately twice as high as that of the diurnal profile. This difference is explained by the fact that the optimal storage capacities for the nocturnal and hybrid profiles are twice as large as that of the diurnal profile. Thus, this table highlights the significant influence of the consumption profile on the optimal configuration of the PV/battery system. It underlines the importance of considering this variable during the sizing process to ensure a system that is both efficient and economically viable. Similar conclusions have been reported in recent studies on standalone renewable energy systems, where the temporal distribution of electricity demand significantly affects storage requirements, system reliability, and overall techno-economic performance (Alhazmi *et al.*, 2024; Mensah, Yorke and Majeed 2024, Lotfy *et al.* 2025).

4.9. Comparison with Results from the Classical Method and HOMER Pro

Table 3 presents the optimal configurations of the PV system with battery storage (SYST_PV_BAT), obtained using three different approaches: the proposed methodology, the classical sizing method, and the HOMER Pro software, for three consumption profiles (diurnal, nocturnal, and hybrid). As it can be observed, the approach developed in this study yields the best results in terms of Levelized Cost of Energy (LCOE), closely followed by HOMER Pro, for all profiles analyzed. In contrast, the classical method results in the highest LCOE, identical for all three profiles. For just one day of autonomy, the LCOE obtained using the classical method is approximately twice as high as that obtained using the proposed approach and HOMER Pro. Compared to the classical method, the new approach reduces the LCOE by 75.60%, 58.53%, and 53.65% for the diurnal, nocturnal, and hybrid profiles respectively. These differences could be even more significant if longer autonomies (e.g., 2 or 3 days), as typically assumed in the classical method, were considered. Compared to HOMER Pro, the proposed method also achieves LCOE reductions of 13.04%, 21.15%, and 23.91% for the diurnal, nocturnal, and hybrid profiles respectively. This difference is not merely the result of parameter tuning, but rather stems from fundamental differences in the optimization frameworks. While HOMER Pro optimizes the system primarily based on the net present cost using aggregated energy balances, the proposed methodology explicitly enforces an annual LPSP constraint and simulates the hourly energy balance over a full year. This allows the sizing process to capture the real temporal mismatch between generation and demand, which is particularly critical for intermittent load profiles. This difference is mainly due to the fact that HOMER Pro does not account for inactive hours (i.e., periods with no power demand) when calculating the average hourly consumption. This omission leads to overestimated storage autonomy or capacity, as shown by the simulation results. In addition, HOMER Pro does not explicitly track the hourly evolution of the battery state of charge (SOC) for the purpose of aging assessment. In contrast, the proposed approach computes the SOC trajectory over the entire year and applies Rainflow cycle counting combined with Miner's rule to identify the actual charge–discharge cycles experienced by the battery. This enables a more realistic estimation of battery lifetime, replacement frequency, and associated costs, which directly affects the LCOE. Thus, the approach developed here appears to be a relevant alternative for sizing stand-alone photovoltaic systems with storage, providing both better technical reliability and improved economic accessibility. Moreover, it directly identifies the optimal series/parallel configuration of PV modules and batteries, thereby delivering the actual sizes to be installed. By contrast, HOMER Pro provides optimal solutions in terms of aggregated capacities (kW and kWh), without explicitly determining the discrete series–parallel configuration of PV modules and batteries. This difference is non-negligible in practical applications, as discrete sizing constraints can significantly influence both investment cost and system performance, especially for small scale standalone systems. This level of detail is not provided by HOMER Pro, which only offers a preliminary sizing. Overall, this comparison confirms that the proposed methodology does not merely reproduce the results of existing tools such as HOMER Pro, but provides a complementary and more physically consistent sizing framework. By explicitly accounting for load intermittency, real battery cycling behavior, and temperature dependent aging, the proposed approach reduces the risk of storage oversizing while maintaining the required supply reliability. In conclusion, this approach can be recommended to designers of stand-alone PV systems with storage in hot climate regions. The LCOE values obtained (0.20–0.41 EURO/kWh) fall within the lower range reported for renewable off-grid electrification systems supplying isolated communities. According to the International Renewable Energy Agency, renewable mini-grids typically exhibit LCOE values between 0.26 and 0. 86 EURO/kWh depending on site conditions and system configurations (International Renewable Energy Agency

Table 3
Optimal Configurations of the SYST_PV_BAT System and Comparison of Sizing Methods

Method	Profile	PV generator Size (Wp)	Storage Capacity (Ah)	Storage Capacity (kWh)	Storage Autonomy	Storage Life time (Years)	Hourly average consunption (Hours)	LPSP (%)	LCOE (EURO/ kWh)
Proposed Method	Diurnal	1060	60	2.88	5 h	13.35	500	1	0.20
	Nocturnal	1060	120	5.76	11 h	7.50	416.67	2.52	0.41
	Hybrid	1060	120	5.76	22 h	10.20	208.33	1.37	0.35
Classical Method	Diurnal	1060	300	14.70	1 day	10	208.33	---	0.82
	Nocturnal	1060	300	14.70	1 day	10	208.33	---	0.82
	Hybrid	1060	300	14.70	1 day	10	208.33	----	0.82
HOMER Pro software	Diurnal	1270	83.33	4	19.7 h	10	208.33	5	0.23
	Nocturnal	1200	166.66	8	39.3 h	10	208.33	5	0.52
	Hybrid	1160	166.66	8	39.3 h	10	208.33	5	0.46

2023). Comparable techno-economic performances have also been reported in recent studies on standalone PV-battery systems, where LCOE values generally range between about 0.30 and 0.60 EURO/kWh depending on system size and local resource availability (Ahmed et al., 2025; Belboul et al., 2024).

5. Conclusion

In this paper, a methodology for the optimal selection and sizing of photovoltaic (PV)/wind systems with battery storage, integrating a predictive battery aging model, was presented and simulated through a case study. Beyond a conventional sizing exercise, this work proposes a comprehensive techno-economic optimization framework based on an hourly simulation approach that explicitly integrates battery cycling aging, thermal effects, reliability constraints (LPSP), and economic performance (LCOE). This framework enables a realistic assessment of both system reliability and long-term cost under real operating conditions. The results obtained were compared with those from the classical intuitive sizing method and the HOMER Pro software, one of the most widely used tools currently available. The chosen study site is Nagréongo, a rural area located about 35 km east of Ouagadougou, Burkina Faso. For the choice of system type, Capacity Factors (CF) and Weighted Index of Complementarity and Productivity (WICP) were evaluated for a range of Aeolos vertical onshore micro-wind turbines, with nominal powers between 0.2 and 1 kW and hub heights ranging from 5 to 80 meters. The results show that, regardless of the turbine power or height, the CF remains below the acceptable threshold of 20%, and the WICP is also below 40%. This indicates low productivity and insufficient complementarity with PV, making the site unsuitable for wind energy. Thus, only a PV/battery system is deemed appropriate. To technically and economically optimize this system, the indicators Loss of Power Supply Probability (LPSP) and Levelized Cost of Energy (LCOE) were used to evaluate, respectively, its reliability and cost. Three hourly daily consumption profiles (Nocturnal, Diurnal, and Hybrid) were studied for three fictitious households, each with a daily energy demand of 5 kWh, to analyze the impact of the load profile on the optimal configuration and LCOE. Battery aging was modeled using the Rainflow algorithm and Miner's rule, considering local climatic conditions. The results also demonstrate that even a moderate deviation from the reference temperature (25 °C) significantly affects battery lifetime and replacement frequency. Neglecting thermal effects would therefore lead to an overestimation of storage lifetime and an underestimation of the real LCOE, especially in hot climates such as sub-Saharan Africa. This confirms that battery aging models calibrated at standard conditions are not sufficient for realistic system optimization in tropical environments. The results show that, although the three households have identical energy demand, their optimal configurations differ due to their hourly consumption profiles. This highlights the importance of considering the load profile in system sizing. The real optimal installed sizes obtained to cover at least 95% of energy needs are:

- Hybrid profile: 1060 Wp and 120 Ah (22 h autonomy), 10.20 years lifetime for storage, LPSP of 1.37%, and LCOE of 0.35 EURO/kWh.
- Nocturnal profile: 1060 Wc and 120 Ah (11 h autonomy), 7.50 years lifetime for storage, LPSP of 2.52%, and LCOE of 0.41 EURO/kWh.
- Diurnal profile: 1060 Wc and 60 Ah (5 h autonomy), 13.35 years lifetime for storage, LPSP of 2.52%, and LCOE of 0.20 EURO/kWh.

A 100% coverage configuration is also possible but requires twice the PV Generator size and storage capacity compared to the 95% coverage setup, which significantly increases the system cost. The comparison with the intuitive method and HOMER Pro software shows that the proposed approach reduces the LCOE by more than 50% compared to the classical method and by about 20% compared to HOMER Pro. Thus, the approach developed here appears to be a relevant alternative for the selection and sizing of autonomous PV and/or wind systems with storage, offering both better technical reliability and improved economic accessibility. Furthermore, it allows direct identification of the optimal series/parallel arrangement of system components (PV modules, micro-wind turbines, and batteries), thereby providing the actual sizes to be installed. These performances are due to the integration of real battery aging and the use of an hourly consumption profile that accounts for both active and inactive hours of the day, enabling precise determination of the required autonomy and finding a good compromise between LPSP and LCOE.

Nevertheless, this study presents some limitations**.** First, the analysis is conducted on a low-wind-potential site, which restricts the assessment of hybrid PV/Wind configurations and limits the conclusions regarding wind energy integration. As a result, the applicability of the proposed methodology to high-wind-potential sites has not been fully explored. Second, the results are based on numerical simulations without experimental validation under real operating conditions.

Although the models used incorporate realistic meteorological data, detailed battery aging mechanisms, and local economic parameters, on-site experimental measurements would further strengthen the reliability of the proposed approach. Future work will therefore focus on applying the methodology to sites with higher wind resources and conducting experimental validation of the PV/battery system performance and battery aging behavior, in order to further enhance the robustness and generalizability of the proposed framework.

Acknowledgements

This work was supported by the Regional Scholarship and Innovation Fund (RSIF) under the Partnership for Skills in Applied Sciences, Engineering and Technology (PASET) initiative. The authors thank the International Centre of Insect Physiology and Ecology (ICIPE) for managing the RSIF fund.

Data availability

Data will be made available on request.

Numenclature

a_r	:	Real interest rate (%)
CRF	:	Capital Recovery Factor (%)
C_{Smod}	:	Specific cost of PV modules (EURO/Wp)
$C_{CONVERT}$	:	Total cost of converters
$C_{SUP-INST-TRANS}$	:	Cost in EURO (support + transport + system installation)
C_{SBAT}	:	Specific cost of batteries (EURO)
C_{IT}	:	Total investment cost (EURO)
C_{OM}	:	Total operation and maintenance cost (EURO)
C_R	:	Total replacement cost of components (EURO)
D_S	:	System lifetime (years)
D_{BAT}	:	Battery lifetime (years)
DOD_{MAX}	:	Maximum depth of discharge of batteries (%)
DOD_j	:	Depth of discharge for each cycle j identified by the Rainflow algorithm
E_D	:	Average daily consumption (Wh/day)
E_{SD}	:	Specific daily energy produced per 1 kW of wind turbine (kWh/kW/day)
E_H	:	Average hourly consumption (Wh/h)
$\eta_{CC/CC}$	:	Charge controller efficiency (%)
η_{BAT}	:	Battery efficiency (%)
N_H	:	Number of autonomy hours (h)
$N_{H_{MAX}}$	:	Maximum autonomy hours set (h)
$\eta_{DC/AC}$	:	Inverter efficiency (%)
CF	:	Wind turbine capacity factor (%)
f_{loss}	:	Soiling factor (%)
F_a	:	Global cost discount factor for operation and maintenance (%)
F_{a_j}	:	Global cost discount factor for replacement of each component j (%)
$G_H(t)$	:	Global solar irradiance measured on horizontal plane (W/m²)
$G_I(t)$	:	Global solar irradiance estimated on tilted plane (W/m²)
G_{ref}	:	Reference solar irradiance (W/m²)
H_{ref}	:	Reference height or hub height of a given wind turbine (m)
TCI	:	Temporal Complementarity Index (%)
$WICP$	:	Weighted Indices of Complementarity and Productivity (%)
I_D	:	Average daily solar irradiation (Wh/m²/day or kWh/m²/day)
i	:	Inflation rate (%)
$LPSP$	:	Loss of Power Supply Probability (%)
$LPSP_{MAX}$	:	LPSP threshold set by the designer
$LCOE$	:	Levelized Cost of Energy (LCOE) (EURO/kWh)
N_{Hoff}	:	Number of non-active hours (zero power demand) in a day
N_D	:	Number of autonomy days (days)
N_{R_j}	:	Number of replacements of each component j
NPV	:	Net Present Value (EURO
μ	:	Maximum energy level not to be exceeded in batteries during charging (%)
PV	:	Photovoltaic
$P_{PV}(t)$	:	Instantaneous power delivered by the PV generator (W)
$P_{WT}(t)$	:	Instantaneous power delivered by the wind generator (W)
$P_{WT}^{norm}(t)$	:	normalized hourly profile of wind production
$P_{PV}^{norm}(t)$	:	normalized hourly profile of solar production
$P_{CH}(t)$	:	Instantaneous power demanded by the user load (W)
P_{mod}	:	Peak power of the selected PV module (Wp
$P_{P_{MIN}}$	:	Minimum threshold of peak power for the PV generator
$P_{P_{MAX}}$	:	Maximum threshold of peak power for the PV generator
P_P	:	Peak power of the PV generator from optimization (Wp)
$P_{P_{INST}}$	:	Real installed optimal peak power of the PV generator (Wp)
P_{WTR}	:	Nominal power of the micro-wind turbines from optimization (W)
$P_{WTR_{UN}}$	:	Nominal power of a micro-wind turbine (W)
$P_{WTN_{INST}}$	:	Real installed optimal nominal power of the wind generator (W)
SOC	:	State of charge of the batteries (Wh)
SOC_{MAX}	:	Maximum state of charge of the battery (Wh)
$SOC(t)$	:	Instantaneous state of charge of the battery (Wh)
SOC_{MIN}	:	Minimum state of charge of the battery (Wh)
S_{BAT}^{CLA}	:	Storage capacity from classical method (Ah)
S_{BAT}	:	Storage capacity from optimization (Ah)
$S_{BAT_{INST}}$	:	Real installed optimal storage capacity (Ah)
$S_{BAT_{UN}}$	:	Storage capacity of one battery (Ah)
T_{mod}	:	Instantaneous PV module temperature (°C)
$T_a(t)$	:	Instantaneous ambient temperature (°C)
T_{ref}	:	Reference ambient temperature or test conditions for modules (°C)
T_{NOCT}	:	PV module temperature under test conditions (800W/m²;20°C)
Ta_{moy}	:	Annual mean hourly ambient temperature (°C)
Ta_{ref}	:	Reference ambient temperature for batteries (°C)
T_{VA}	:	Annual battery aging rate (%)
$U_{BAT_{UN}}$	:	Battery terminal voltage (V)
U_{BAT}	:	Battery bank terminal voltage (V)
U_{SYST}	:	System operating voltage (V)
$U_{WT_{UN}}$	:	Wind turbine terminal voltage (V)
v	:	Wind speed measured at a site and height H (m/s)
v_{IN}	:	Wind turbine cut-in speed (m/s)
v_R	:	Wind turbine nominal speed (m/s)
v_{OUT}	:	Wind turbine cut-out speed (m/s)

References

Andrenacci, N.; Vellucci, F.; Sglavo, V. (2021) The Battery Life Estimation of a Battery under Different Stress Conditions. *Batteries,* 7, 88. https://doi.org/10.3390/batteries7040088

Aza-Gnandji, M. R., Fifatin, F. X., Hounnou, A. H. J., Dubas, F., Chamagne, D., Espanet, C., … & Vianou, A. (2018). Complementarity between Solar and Wind Energy Potentials in Benin Republic. *Advanced Engineering Forum*, 28, 128-138. https://doi.org/10.4028/www.scientific.net/aef.28.128

Alhazmi, M., Alfadda, A., & Alfakhri, A. (2024). Analysis of a grid-connected solar PV system with battery energy storage for irregular load profile. *Energies*, 17(14), 3463. https://doi.org/10.3390/en17143463.

Ahmed, A., Bello, A., A., Habou, D. (2013). An Evaluation of Wind Energy Potential in the Northern and Southern Regions of Nigeria on the Basis of Weibull and Rayleigh Models. *American Journal of Energy Engineering*, *1*(3), 37-42. https://doi.org/10.11648/j.ajee.20130103.11

Ahmed, A. A., Didane, D. H., Hussein, B. A., Al-Alimi, S., Manshoor, B., & Saif, Y. (2024). Techno-Economic Analysis of Off-Grid PV Solar System for Residential Building Load: A Case Study in Baidoa, Somalia. *International Journal of Integrated Engineering*, *16*(1), 178-188. https://publisher.uthm.edu.my/ojs/index.php/ijie/article/view/14217

Bakelli, Y., Kaabeche, A., Hechaichi, A. & Elbachir, M.I. (2025). A Comparative Study Between Autonomous Photovoltaic Systems Sizing Methods. In: Guerri, O., Arab, A.H., Imessad, K. (eds) Technological and Innovative Progress in Renewable Energy Systems. *Advances in Science, Technology & Innovation*. Springer, Cham. https://doi.org/10.1007/978-3-031-71926-4_14

Belboul, Z., Toual, B., Bensalem, A., Ghenai, C., Khan, B., Kamel, S. (2024) Techno-economic optimization for isolated hybrid PV/wind/battery/diesel generator microgrid using improved salp swarm algorithm. *Scientific Reports* 14, 2920. https://doi.org/10.1038/s41598-024-52232-y

Boumechta, S. & Kaabeche A. (2015) Optimisation du dimensionnement d'un système hybride Eolien/Diesel, *Journal of Renewable Energies,* 18(3), 439-456 https://doi.org/10.54966/jreen.v18i3.519

Busaidi, A.S. A., Kazem, H.A., Badi, A.H. A. & Khan, M.F. (2016) A review of optimum sizing of hybrid PV–Wind renewable energy systems in Oman. *Renewable and Sustainable Energy Reviews,* 53, 185-193 ; https://doi.org/10.1016/j.rser.2015.08.039.

Brenna, M., Lazaroiu, G. C. & Tironi, E.(2006). High power quality and DG integrated low voltage dc distribution system, *2006 IEEE Power Engineering Society General Meeting*, Montreal, QC, Canada, DOI**:** 10.1109/PES.2006.1709440

Bhatia, A. (2008), Design and Sizing of Solar Photovoltaic Systems – R08-00, An online course brought by Continuing Education and Development (CED). Available on mine https://www.cedengineering.com/userfiles/R08-002%US.pdf

Beluco, A., De Souza, P. k. & Krenzinger, A. (2008), A dimensionless index evaluating the time complementarity between solar and hydraulic energies, *Renewable Energy*, 33(10), 2157–2165. https://doi.org/10.1016/j.renene.2008.01.019

Cardona, M.S.D. & López, L. M. (1998) A simple model for sizing stand-alone photovoltaic systems, *Solar Energy Materials and Solar Cells*, 55(3), 199-214; https://doi.org/10.1016/S0927-0248(98)00093-2

Carta, J.A., Ramírez, P. &Velázquez, S. (2009) A review of wind speed probability distributions used in wind energy analysis: Case studies in the Canary Islands, *Renewable and Sustainable Energy Reviews,*13(5), 933-955, https://doi.org/10.1016/j.rser.2008.05.005

Canales, FA., Jurasz, J., Beluco, A. & Kies, A. (2019) Assessing temporal complementarity between three variable energy sources by means of correlation and compromise programming, *Energy*, 192, 116637; https://doi.org/10.1016/j.energy.2019.116637

Diouf, B. & Miezan, E. (2024) Unlocking the Technology Potential for Universal Access to Clean Energy in Developing Countries. *Energies*,17(6),1488; https://doi.org/10.3390/en17061488

Diaf, S., Notton, G., Belhamel, M., Haddadi, M., Louche, A. (2008) Design and techno-economical optimization for hybrid PV/wind system under various meteorological conditions, *Applied Energy,* 85(10), 968–987; https://doi.org/10.1016/j.apenergy.2008.02.012

Diaf, S., Belhamel M., Haddadi M., Louche A. (2008). Technical and economic assessment of hybrid photovoltaic/wind system with battery storage in Corsica Island. *Energy Policy*, 36(2), 743e54; https://doi.org/10.1016/j.enpol.2007.10.028

Derai, S. A. & Kaabeche, A. (2016) Modélisation et dimensionnement d'un système hybride Eolien/ Photovoltaïque autonome, *Journal of Renewable Energies*, 19(2), 265 - 276, https://doi.org/10.54966/jreen.v19i2.566

DiOrio, N., Dobos, A., & Janzou, S., Austin, N., Blake,L. (2015). Techno-economic modeling of battery energy storage in SAM. (National Renewable Energy Laboratory) NREL, Technical Report NREL/TP-6A20-64641. https://doi.org/10.2172/1225314

Du, H., Wang, Y., Kang, Y., Zhao, Y., Tian, Y., Wang, X,.Tan,Y., Liang, Z., Wozny,J., Li,T., Ren, D., Wang, L., He, H., Xiao, P., Mao, E., Tavajohi, N., Kang, F., Li, B. (2024). Side Reactions/Changes in Lithium-Ion Batteries: Mechanisms and Strategies for Creating Safer and Better Batteries, *Advanced materials*, 36(29), 2401482**.** https://doi.org/10.1002/adma.202401482

Fouzia, B. (2023) Technico-economical efficient multiyear comparative analysis of temperature and cycling effect on Li-ion and lead-acid batteries — A case study, *Journal of Energy Storage*, 74(Part B), 109310 ; https://doi.org/10.1016/j.est.2023.109310

Gbadegesin, A.,O., Sun, Y., Nwulu,N.,I. (2019). Techno-economic analysis of storage degradation effect on levelised cost of hybrid energy storage systems, *Sustainable Energy Technologies and Assessments*, 36, 100536, https://doi.org/10.1016/j.seta.2019.100536

Global Wind Energy Council (2024), GLOBAL WIND REPORT 2024, published 16 April 2024, Available online. Accessed on 3 march 2025. https://www.gwec.ne.

HOMER Energy by UL (2023). HOMER Pro User Manual v3. Available on https://www.homerenergy.com/products/pro/docs/index.html. Accessed on 3 March 2025

Heide, D., von Bremen, L., Greiner, M., Hoffmann, C., Speckmann, M., & Bofinger, S. (2010). Seasonal optimal mix of wind and solar power in a future, highly renewable Europe. *Renewable Energy,* 35(11), 2483–2489. https://doi.org/10.1016/j.renene.2010.03.012

Halabi, L. M., Mekhilef, S., Olatomiwa, L., & Hazelton, J. (2017). Performance analysis of hybrid PV/diesel/battery system using HOMER: A case study Sabah, Malaysia, *Energy* Conversion and Management, 144, 322–339. https://doi.org/10.1016/j.enconman.2017.04.070

International Energy Agency (2024). *World Energy Outlook 2024*, International Energy Agency (IEA), Paris, Licence : CC BY 4.0 (rapport); CC BY NC SA 4.0.(Annex A), https://www.iea.org/reports/world-energy-outlook-2024. Accessed on 7 March 2025.

International Energy Agency (2024). SDG7: Data and projections, IEA, Paris, Licence: CC BY 4.0, https://www.iea.org/reports/sdg7-data-and-projections. Available on line. Accessed on 7 March 2025.

International Energy Agency (2024). World Energy Outlook Special Report Africa Energy Outlook 2022, 2022. [Online]. Available: www.iea.org/t&c/

Ishaq, S., Khan, I., Rahman, S., Hussain, T., Iqbal, A., Elavarasan, R.M. (2022) A review on recent developments in control and optimization of micro grids. *Energy Report*, *8*, 4085–4103. https://doi.org/10.1016/j.egyr.2022.01.080

IRENA (2023), Renewable energy for remote communities: A guidebook for off-grid projects, International Renewable Energy Agency (IRENA), Abu Dhabi. Available for download on: www.irena.org/publications.

Jonasson, E., & Temiz, I. (2025). Evaluating complementarity: A review of metrics and their implications for hybrid renewable energy systems. *Renewable and Sustainable Energy Reviews*, 226, 116422. https://doi.org/10.1016/j.rser.2025.116422

Jurasz, J., Guezgouz, M., Campana, P.E., Kazmierczak, B., Kuripi, A., Bloomfield, H., Hingray, B., Canales, F.A., Hunt, J.D., Sterl, S., Elkadeem, M.R.(2024) Complementarity of wind and solar power in North Africa: Potential for alleviating energy droughts and impacts of the North Atlantic Oscillation, *Renewable and Sustainable Energy Reviews*; https://doi.org/10.1016/j.rser.2023.114181

Jurasz, J., Bochenek, B., Wieczorek, J., Jaczewski, A., Kies, A., Figurski, M. (2025) Energy potential and economic viability of small-scale wind turbines, *Energy*, 322, 135608, https://doi.org/10.1016/j.energy.2025.135608

Jurasz, J., Canales, FA., Kies, A., Guezgouz, M., Beluco, A. (2019), A review on the complementarity of renewable energy sources: concept, metrics, application and future research directions. *Solar Energy,* 195, 703-724. https://doi.org/10.1016/j.solener.2019.11.087

Kafando, J.G., Yamegueu, D., Houdji, E.T.(2024) Review on Sizing and Management of Stand-Alone PV/Wind Systems with Storage, *Heliyon,* 10 (18), e38080; https://doi.org/10.1016/j.heliyon.2024.e38080

Kaabeche, A., Belhamel, M., Ibtiouen, R. (2011)Sizing optimization of grid-independent hybrid photovoltaic/wind power generation system, *Energy,* 36 (2), 1214–1222, https://doi.org/10.1016/j.energy.2010.11.024

Kim S., H., Shin,Y., J. (2023). Optimize the operating range for improving the cycle life of battery energy storage systems under uncertainty by managing the depth of discharge, *Journal of Energy Storage*, 73(Part D), 109144. https://doi.org/10.1016/j.est.2023.109144

Kotb, K.M., Elkadeem, M.R., Elmorshedy, M.F., Dán, A. (2020) Coordinated power management and optimized techno-enviro-

economic design of an autonomous hybrid renewable microgrid: a case study in Egypt, *Energy Conversion and Management,* 221 , https://doi.org/10.1016/j.enconman.2020.113185

Korsaga, E., Koalaga, Z., Bonkougou, D., Zougmoré, F. (2018) Comparaison et détermination des dispositifs de stockage appropriés es pour un système photovoltaïque autonome en zone sahélienne, *Journal International de Technologie, de l'Innovation, de la Physique, de l'Energie et de l'Environnement*, 4, 2428–8500, http://dx.doi.org/10.18145/jitipee.v4i1.161

Konate, S. (2025), Guide technique sur l'électrification au solaire photovoltaïque des établissements de santé en milieu rural d'Afrique subsaharienne. Étude réalisée pour l'Alliance for Rural Electrification et soutenue par l'ADEME. https://www.ruralelec.org/wp-content/uploads/2025/06/Guide-technique-sur-lelectrification-des-etablssements-de-sante-en-milieu-rural.pdf

Lv, F. and Tang, H.(2025) Assessing the impact of climate change on the optimal solar–wind hybrid power generation potential in China: A focus on stability and complementarity, *Renewable and Sustainable Energy Reviews,* 212, 115429, https://doi.org/10.1016/j.rser.2025.115429

Layadi, T. M. & Champenois, G. (2014) Etude du vieillissement d'un banc de stockage plomb acide dans un système hybride multi-sources. Symposium de Génie Électrique 2014, Cachan, France. https://hal.science/hal-01065201v1

Leng, F., Tan, C., M. & Pecht, M. (2015). Effect of Temperature on the Aging rate of Li Ion Battery Operating above Room Temperature. *Scientific Reports* , 5,12967; https://doi.org/10.1038/srep12967

Lotfy, A., Anis, W., R., Newagy, F., Mohamed, S., M. (2025**)** Comparative Designs for Standalone Critical Loads Between PV/Battery and PV/Hydrogen Systems, *Hydrogen*, *6*(3), 46; https://doi.org/10.3390/hydrogen6030046

Madani, S.S., Shabeer, Y., Allard, F., Fowler, M., Ziebert, C., ang, Z., Panchal, S., Chaoui, H., Mekhilef, S., Dou, S.X., (2025). A Comprehensive Review on Lithium-Ion Battery Lifetime Prediction and Aging Mechanism Analysis. *Batteries* 11(4), 127. https://doi.org/10.3390/batteries11040127

Moussa Kadri, S., Dakyo, B., Camara, M.B., Coulibaly, Y. (2022) Hybrid Diesel/PV Multi-Megawatt Plant Seasonal Behavioral Model to Analyze Microgrid Effectiveness: Case Study of a Mining Site Electrification. *Processes,* 10, 2164. https://doi.org/10.3390/pr10112164

Mehallou, A., M'hamdi, B., Amari, A., Teguar, M., Rabehi, A., Guermoui, M., Alharbi, A.H., El-kenawy, E. M.& Kafhaga, D.S. (2025) Mult objective design of an autonomous hybrid renewable energy system in the Adrar Region, Algeria, *Scientific Reports* ,15, 4173 https://doi.org/10.1038/s41598-025-88438-x

Mensah, S., A., Yorke, F., O., Majeed, I., B. (2024). Evaluating the impact of industrial loads on the performance of solar PV/diesel hybrid renewable energy systems for rural electrification in Ghana. *Energy Conversion and Management: X*, 21, 100525. https://doi.org/10.1016/j.ecmx.2024.100525.

Nationally Determined Contributions (2024). Nationally Determined Contributions (NDCs) synthesis report ; https://unfccc.int/process-and-meetings/the-paris-agreement/nationally-determined-contributions-ndcs. Available on line. Accessed on 7 March 2025.

Nsouandélé, J.L., Kidmo, D.K., Djetouda, S.M. & Djongyang, N. (2017) Estimation statistique des données du vent à partir de la distribution de Weibull en vue d'une prédiction de la production de l'énergie électrique d'origine éolienne sur le Mont Tinguelin à Garoua dans le Nord Cameroun, *Journal of Renewable Energies*, 19(2), 291–301; https://doi.org/10.54966/jreen.v19i2.568

Othman, Z., Sulaiman, S. I., Musirin, I., Omar, A. M. & Shaari S. (2022) Handling multiple models of system components in stand-alone photovoltaic system sizing via iterative sizing algorithm, *Energy Reports*, 8, 674-680. https://doi.org/10.1016/j.egyr.2022.10.178

Olomiyesan, B., Oyedum, O., Ugwuoke, P., & Abolarin, M. (2017). Assessment of wind energy resources in Nigeria: a case study of north-western region of Nigeria. *International Journal of Physical Research*, *5*(2), 83-90. https://doi.org/10.14419/ijpr.v5i2.8327

Ohunakin, O.S., Oyewola, O.M. & Adaramola, M.S. (2013). Economic analysis of wind energy conversion systems using levelized cost of electricity and present value cost methods in Nigeria. *Int J Energy Environ Eng,* 4(2). https://doi.org/10.1186/2251-6832-4-2

Onyeanusi, N.B. (2025). Energy Access Implications for Unserved Communities in Sub-Saharan Africa: Challenges and Opportunities. In: Narra, MM., Narra, S. (eds) African Green Transition Through Innovative Pathways. *World Sustainability Series*. Springer, Cham. https://doi.org/10.1007/978-3-031-87043-9_9

Ren G., Wang, W., Wan , J., Hong , F., Yang, K . (2023). A novel metric for assessing wind and solar power complementarity based on different fluctuation states and amplitudes. *Energy Conversion and Management,* 278, 116721. https://doi.org/10.1016/j.enconman.2023.116721

Ridha, S. H. M., Gomes. C., Hizam, H., Ahmadipour, M., Muhsen, D. H., and Ethaib, S. (2020) Optimum design of a standalone solar photovoltaic system based on novel integration of iterative-PESA-II and AHP-VIKOR Methods, *Processes*, 8(3), https://doi.org/10.3390/pr8030367.

Saxena, S., Le Floch, C., MacDonald, J., & Moura, S. (2015). Quantifying EV battery end-of-life through analysis of travel needs with vehicle powertrain models. *Journal of Power Sources*, 282, 265-276. https://doi.org/10.1016/j.jpowsour.2015.01.072

Sedaghat, A., Alkhatib, F., Eilaghi, A., Mehdizadeh, A., Borvayeh, L., Mostafaeipour, A., Hassanzadeh, A. & Jahangiri, M. (2020) Optimization of capacity factors based on rated wind speeds of wind turbines, *Energy Sources, Part A: Recovery, Utilization, and Environmental Effects,* 46(1), 6104-6125 https://doi.org/10.1080/15567036.2020.1740834

Shen, W., Dong, J., Lu, Y., Yan, K., Guan, Y., Zhao, G., Li, B., Wang, X., Tang, R., Zhou, J., Li, N., Su, Y., Wu, F. & Chen, L. (2025). Coupled influence of state-of-charge and storage temperature on calendar aging and subsequent cycle degradation in $LiFePO_4$/graphite pouch cells. *Journal of Materials Chemistry A,* 13, 26297-26309. https://doi.org/10.1039/D5TA03813H

Solomon, A. A., Child, M., Caldera, U., Breyer, C. (2020). Exploiting wind-solar resource complementarity to reduce energy storage need. *AIMS Energy*, 8(5), 749-770. https://doi.org/10.3934/energy.2020.5.749

United Nations. (2025), UN Sustainable Development Goals. Available on line. Accessed on 7 March 2025. https://sdgs.un.org/goals/goal7.

Witharama, W. M. N., Bandara, K. M. D. P., Azeez, M. I., Bandara,K., Logeeshan,V. and Wanigasekara, A. (2024) Advanced Genetic Algorithm for Optimal Microgrid Scheduling Considering Solar and Load Forecasting, Battery Degradation, and Demand Response Dynamics, *IEEE Access,* 12, 83269-83284.https://doi.org/10.1109/ACCESS.2024.3412914

Yamegueu, D., Nelson, H.T. & Boly, A.S. (2024) Improving the performance of PV/diesel microgrids via integration of a battery energy storage system: the case of Bilgo village in Burkina Faso. *Energy Sustainability and Society*. 14, 48. https://doi.org/10.1186/s13705-024-00480-1

APPENDICES

Appendix A: SERIES/PARALLEL ARRANGEMENT OF COMPONENTS

In order to obtain an optimally configured system that can be actually implemented based on the system's operating voltage and the actual characteristics of the selected modules and batteries, equations (A.1), (A.2), and (A.3) were used to determine the number of PV modules, micro-wind turbines, and batteries to be connected in series, respectively, to reach the system's operating voltage.

$$N_{\mathrm{mod}\_serie} = \frac{U_{SYST}}{U_{\mathrm{mod}}} \quad \text{(A.1)}$$

$$N_{WT\_serie} = \frac{U_{SYST}}{U_{WT_{UN}}} \quad \text{(A.2)}$$

$$N_{BAT\_serie} = \frac{U_{SYST}}{U_{BAT_{UN}}} \quad \text{(A.3)}$$

For the parallel arrangement, equations (A.4), (A.5), and (A.6) were used to determine the respective numbers of strings of PV modules, micro-wind turbines, and batteries to be actually installed, allowing for a slight oversizing or undersizing of ±5% relative to the optimized values of P_P, P_{WTR} and S_{BAT}.

$$N_{\mathrm{mod}\_parallel} = \frac{P_P}{P_{\mathrm{mod}}} \frac{1}{N_{\mathrm{mod}\_Serie}} \quad \text{(A.4)}$$

$$N_{BAT\_parallel} = \frac{S_{BAT}}{S_{BAT_{UN}}} * \frac{1}{N_{BAT\_serie}} \quad \text{(A.5)}$$

$$N_{WT\_parallel} = \frac{P_{WTR}}{P_{WTR_{UN}}} \frac{1}{N_{WT\_Serie}} \quad \text{(A.6)}$$

The actual or real optimal peak power of the PV generator, the actual optimal nominal power of the wind generator, and the actual optimal storage capacity are given respectively by equations (A.7), (A.8), and (A.9):

$$P_{P_{INST}} = N_{\mathrm{mod}\_serie} * N_{\mathrm{mod}\_parallel} * P_{\mathrm{mod}} \quad \text{(A.7)}$$

$$P_{WTR_{INST}} = N_{WT\_serie} * N_{WT\_parallel} * P_{WTR_{UN}} \quad \text{(A.8)}$$

$$S_{BAT_{INST}} = N_{BAT\_serie} * N_{BAT\_parallel} * S_{BAT_{UN}} \quad \text{(A.9)}$$

Appendix B: Description of other proposed algorithms

B.1. Description of ALGO_PV_BAT

The ALGO_PV_BAT algorithm is designed to determine the optimal sizing of an autonomous photovoltaic system with battery energy storage by jointly minimizing the Loss of Power Supply Probability (LPSP) and the Levelized Cost of Energy (LCOE), while explicitly accounting for battery aging.This ALGO_PV_BAT, whose flowchart is presented in Figure 4 proceeds in six step as follows:

Step 1: Definition of the optimization variables and constraints

The optimization is carried out over two main design variables:

- The storage autonomy duration $N_H \in [1, N_{H_{MAX}}]$ (in hours) where $N_{H_{MAX}}$ is user-defined bound.
- The peak power of the PV generator P_P (in kW), varying within: $P_P \in [P_{P_{MIN}}, P_{P_{MAX}}]$ where $P_{P_{MIN}}, P_{P_{MAX}}$ are bounds and expressed by equations 39 and 40

The system is subject to a reliability constraint expressed through the LPSP in %:

($LPSP_{MAX}$ is a predefined admissible threshold)

Step 2: Iterative sizing process

For a given storage autonomy N_H, the corresponding nominal battery capacity S_{BAT} is first computed using equation 6. Then, for this fixed autonomy value, the PV peak power P_P is progressively increased from $P_{P_{MIN}}$ to $P_{P_{MAX}}$

Step 3: Annual system simulation and reliability assessment

For each (N_H, P_P) configuration, the system is simulated over one full year with an hourly time step (t=1,…,8760).

At each time step:

- PV power production $P_{PV}(t)$ is calculated based on solar irradiance and module temperature.
- Battery state of charge $\mathrm{SOC}(t)$ is updated according to the energy balance
- Loss of Power Supply (LPS) is computed whenever the load demand cannot be met.

The $LPSP$ is then evaluated. If $LPSP \geq LPSP_{MAX}$ the algorithm increases P_P and repeats the simulation.

Step 4: Battery aging and lifetime estimation

Once the LPSP constraint is satisfied, the battery aging process is evaluated.

- The depth of discharge (DoD) profile is extracted from the SOC time series.
- Cycle counting is performed using the Rainflow algorithm.
- The equivalent number of cycles is converted using Miner's rule into battery lifetime D_{BAT} (in years), accounting for operating temperature effects.

Step 5: Energy production and economic evaluation

For each feasible configuration, the following indicators are computed:

- Number of battery replacements over the project or system lifetime d (years) (equation 33):
- Levelized Cost of Energy using equation 25:

The result ($N_H, P_P, P_{P_{INST}}, LPSP, D_{BAT} and\ LCOE$) are stored where $P_{P_{INST}}$ is the real optimal peak power of the PV generator got from equation A.7 in Appendix A.

Step 6: Global optimization and selection of the optimal configuration

After repeating the procedure for all autonomy values, the algorithm identifies the optimal configuration by solving the following objective optimization problem:

Min (LCOE) subject to $LPSP \leq LPSP_{MAX}$

The configuration that offers the best compromise between system reliability and economic performance is retained as the optimal PV–battery system.

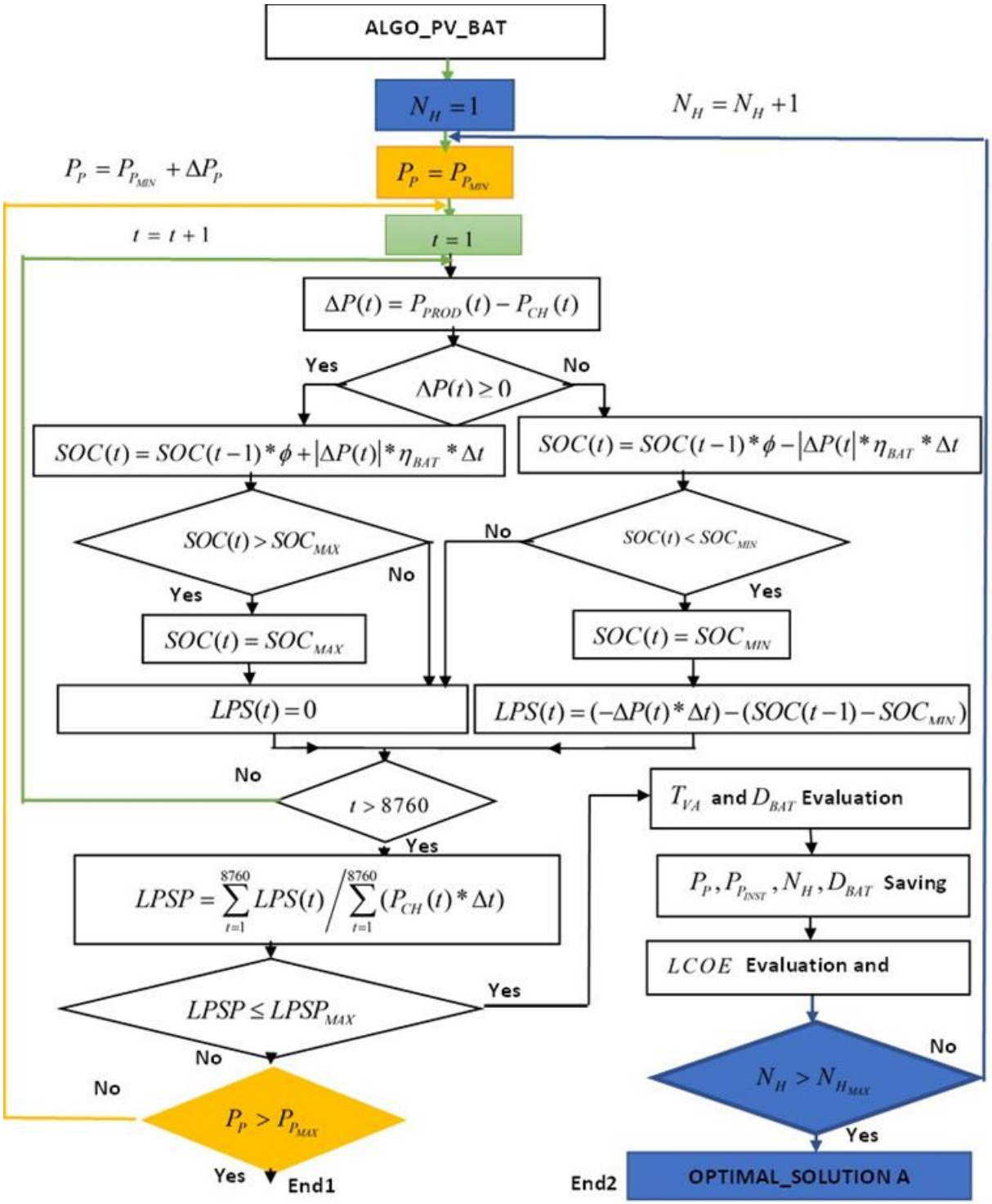

Figure B1. Flowchart of ALGO_PV_BAT.

B.2.Description of ALGO_EOL_BAT

The ALGO_EOL_BAT, whose flowchart is presented in Figure 5, follows the same principle (six steps) as the ALGO_PV_BAT. However, in this case, it is the rated power of the wind generator P_{WTR}, that is iterated for each value of storage autonomy duration. The rated power of the wind generator P_{WTR} (in kW), varying within: $P_{WTR} \in [P_{WTR_{MIN}}, P_{WTR_{MAX}}]$ where $P_{P_{MIN}}, P_{P_{MAX}}$ are bounds and expressed by equations 41 and 42.

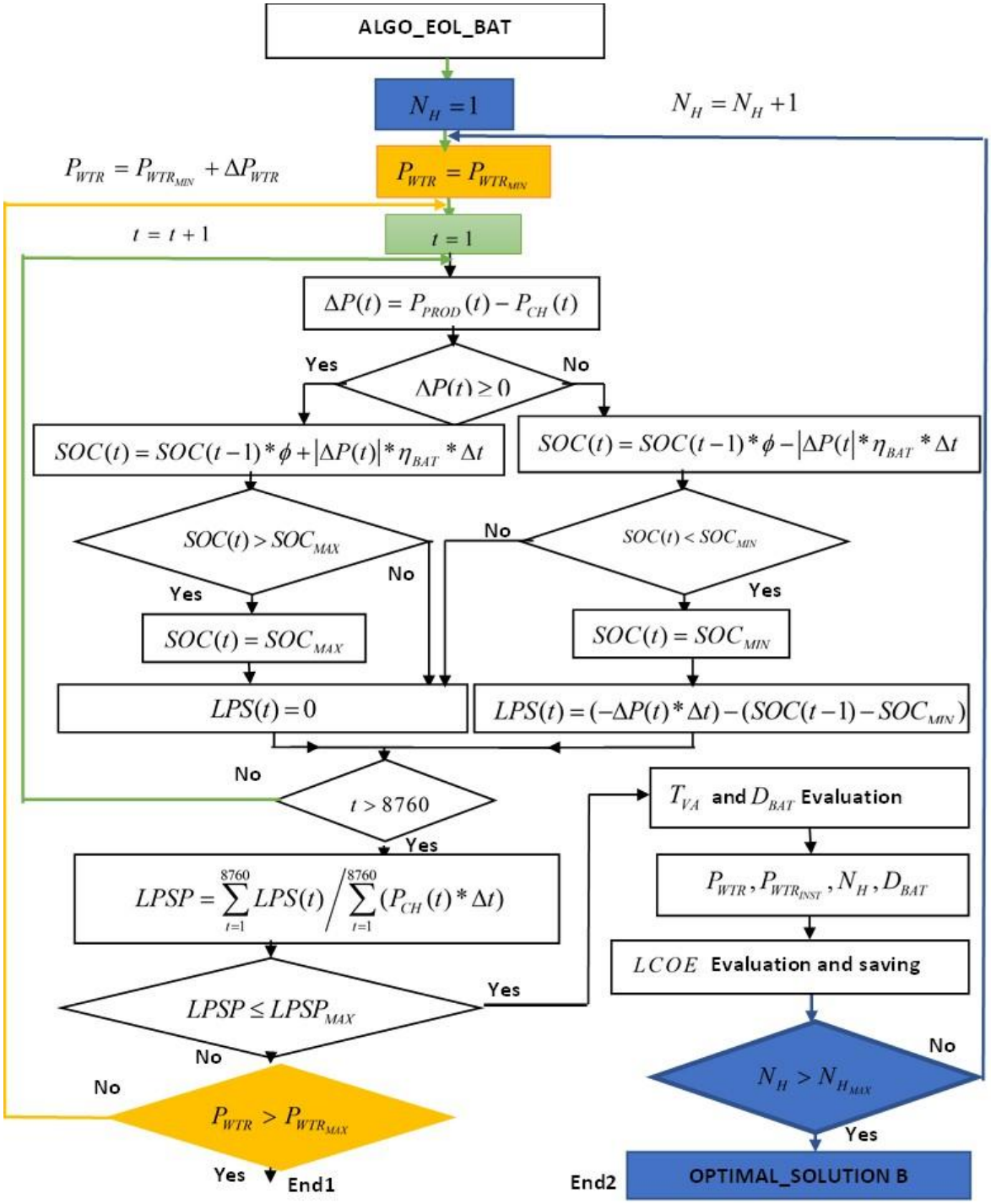

Figure B2. Flowchart of ALGO_EOL_BAT

B.3. Description of ALGO_PV_EOL_BAT

The hybrid PV/Wind/Battery system sizing is performed using an iterative optimization algorithm, denoted ALGO_PV_EOL_BAT, whose flowchart is shown in Figure 6. The objective of the algorithm is to identify the optimal combination of photovoltaic peak power, wind turbine rated power, and battery capacity that satisfies a predefined reliability constraint while minimizing the levelized cost of energy (LCOE). The optimization proceeds in six step as follows:

Step 1: Selection of the Wind Turbine Based on Complementarity

The optimization process starts with the selection of a micro-wind turbine whose rated power P_{WTR} ensures an acceptable compromise between wind energy productivity and its complementarity with solar energy. This selection is guided by the Weighted Index of Complementarity and Productivity (WICP), defined in the methodology section. The wind turbine is retained when: $WICP \geq WICP_{t\arg et} = 40\%$

Once the rated wind power P_{WTR} satisfying this criterion is identified, it is fixed for the remainder of the optimization process.

Step 2: Iterative Sizing of the Photovoltaic Generator and Battery Autonomy

For a given storage autonomy N_H, the corresponding nominal battery capacity S_{BAT} is first computed using equation 6. Then, for this fixed autonomy value, the PV peak power P_P is iteratively increased, starting from a minimum admissible value $P_{P_{MIN}}$ according to:

$P_P = P_{P_{MIN}} + \Delta P_P$ where ΔP_P is the incremental step.

For each candidate configuration, an hourly simulation over one full year (t=1,…,8760) is performed.

Step 3: Hourly Energy Balance and Battery State of Charge

At each time step t, the net power balance is computed as:

$\Delta P = P_{PROD}(t) - P_{CH}(t)$

Where $P_{PROD}(t)$ is the total power generated by the PV and wind subsystems, and $P_{CH}(t)$ is the load demand.

The battery state of charge (SOC) is then updated according to the charging mode ($\Delta P(t) > 0$) and discharging mode ($\Delta P(t) < 0$)

The SOC is constrained within operational limits: $SOC_{MIN} \leq SOC(t) \leq SOC_{MAX}$

Step 4: Loss of Power Supply and Reliability Constraint

When the SOC reaches its minimum allowable value and the load demand cannot be fully satisfied, the Loss of Power Supply (LPS) is computed all over the year and the annual Loss of Power Supply Probability (LPSP) **is** then evaluated.

The configuration is considered acceptable only if: $LPSP \leq LPSP_{MAX}$

Step 5: Battery Lifetime and Economic Evaluation

For each acceptable configuration, the battery lifetime D_{BAT} is estimated using the Rainflow cycle-counting algorithm combined with Miner's rule, applied to the hourly SOC profile. The number of battery replacements over the project lifetime is then deduced and the Levelized Cost of Energy (LCOE) is subsequently calculated by accounting for investment costs, replacement costs, operation and maintenance costs and total energy production.

All acceptable configurations are stored along with their corresponding parameters: P_{WTR} P_P, N_H, D_{BAT}, $LPSP$ and $LCOE$

Step 6: Global Optimization Criterion

The optimization process is repeated for increasing values of storage autonomy N_H until the maximum admissible autonomy $N_{H_{MAX}}$ is reached.

Among all stored configurations satisfying the reliability constraint, the optimal solution is selected as the one providing the best techno-economic trade-off, defined as:

Min (LCOE) subject to $LPSP \leq LPSP_{MAX}$

The retained configuration constitutes the optimal hybrid PV/Wind/Battery system, ensuring both high reliability and minimum energy cost under realistic operating conditions.

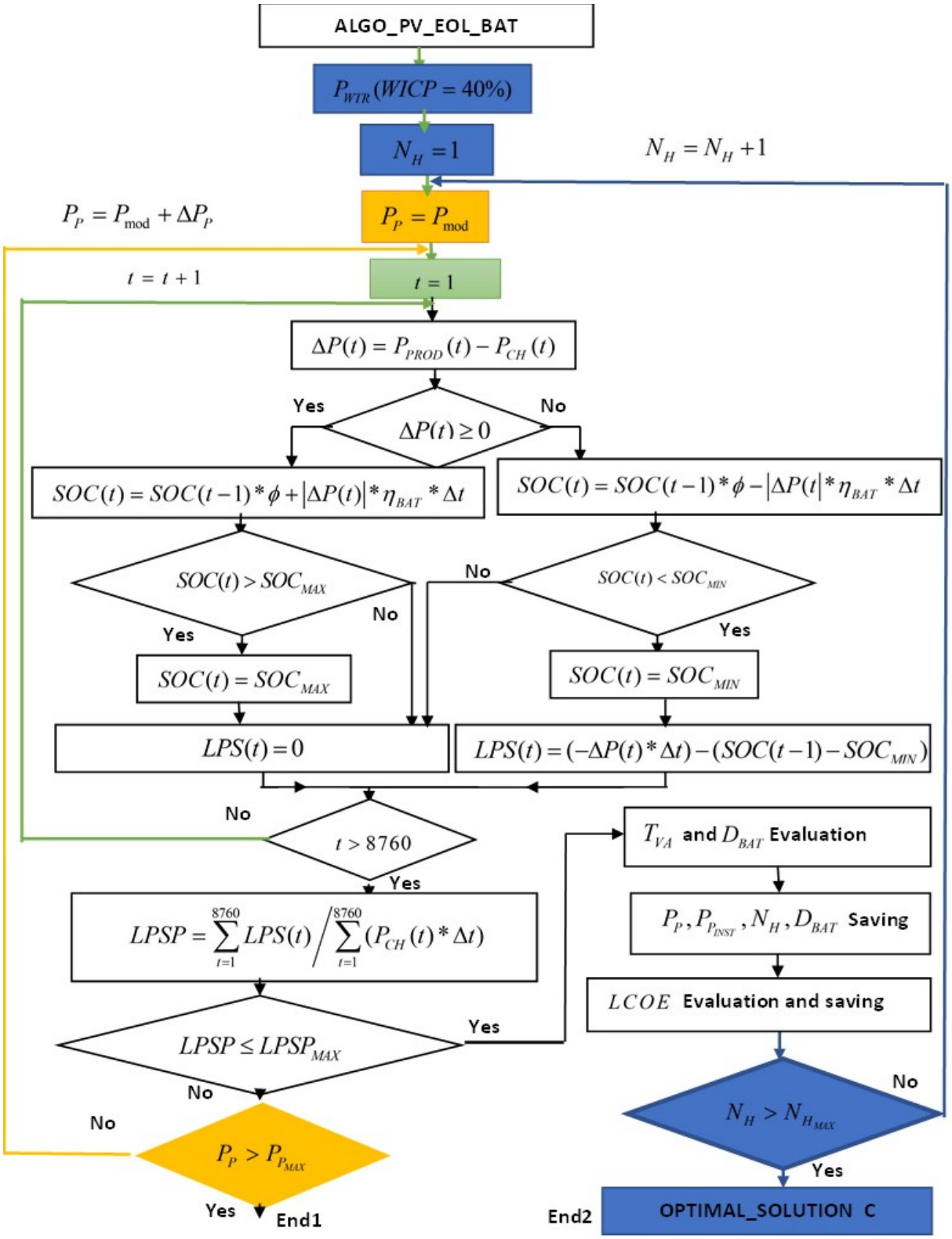

Figure B3. Flowchart of ALGO_PV_EOL_BAT

Appendix C: Others Tables

Theses tables (Table C1, Table C2 and Table C3) presented techno-economic characteristics of system components and optimization constraints also used as the proposed sizing model input parameters in this study.

Table C1. Characteristics, Costs, and Lifespans of System Components

Component**/system**	**Technical Characteristics**	**Unit Cost (EURO)**	**Life time(years)**	**Efficiency (%)**
Polycrystalline PV Module	12V/265W	106.72	20	
Lithium Superspack Battery	12V/60Ah	411.62	To calculate	85
PWM Charge Controlle	48V/30A	91.47	10	90
Inverter (DC/AC)	48V/1200 W et 230V AC /50HZ	414.67	10	95
Horizontal-Axis Wind Turbine	48V/600W	2744.11	20	
System	------	---	20	

Table C2. Technical Specifications of the Wind Turbines

Type of Turbine	**Characteristics**	**Values**
Aeolos Vertical Turbine (48V)	P_{WTR} (Rated power range in kW)	0.2 - 1
	v_{IN} (Cut-in wind speed in m/s)	1.5
	v_R (Rated wind speed in m/s)	10
	v_{OUT} (Cut-out wind speed in m/s)	45
	H (Hub height considered in m)	5 - 80

Table C3. Technical Constraints for Optimization

Parameters	**Values**
$LPSP_{MAX}$ (Maximum allowable Loss of Power Supply Probability in %)	0,5,10
DOD_{MAX} (Maximum allowable battery depth of discharge in %)	80
SOC_{MAX} (Maximum allowable battery state of charge in %)	90
$N_{H_{MAX}}$ (Maximum battery autonomy in hours)	72
ΔP_P (PV generator sizing step in Wc)	265
ΔP_{WTR} (Wind turbine sizing step in W)	200